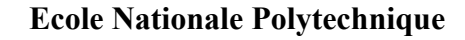
REPUBLIQUE ALGERIENNE DEMOCRATIQUE ET POPULAIRE

Ministère de l'Enseignement Supérieur et de la Recherche Scientifique





Département de génie des matériaux

Centre de Recherche Nucléaire de Draria



End-of-study project dissertation

for obtaining the State Engineer's degree in material engineering

Impact of a Beryllium Deposition on the Reliability of Zircaloy-4/Zircaloy-4
Welds for Fuel Rods in Research Reactors (HMWRR)

Presented by:

Soundousse Nadjlaa TAYSSIR

Supervised by:

Pr. Laribi MERZAK ENP

Dr. Amane SAHLI CRND

Presented and publicly defended on july 08, 2025

Members of the jury:

Chair: Dr. Soumia MERMOUL ENP

Examiner: Dr. Oussama DJEMA CRTSE

Dr. Youssef LARBAH CRNA

Guest: Mr. Omar MENCHI CRND

ENP 2025

REPUBLIQUE ALGERIENNE DEMOCRATIQUE ET POPULAIRE

Ministère de l'Enseignement Supérieur et de la Recherche Scientifique





Département de génie des matériaux

Centre de Recherche Nucléaire de Draria



End-of-study project dissertation

for obtaining the State Engineer's degree in material engineering

Impact of a Beryllium Deposition on the Reliability of Zircaloy-4/Zircaloy-4
Welds for Fuel Rods in Research Reactors (HMWRR)

Presented by:

Soundousse Nadjlaa TAYSSIR

Supervised by:

Pr. Merzak LARIBI ENP

Dr. Amane SAHLI CRND

Presented and publicly defended on july 08, 2025

Members of the jury:

Chair: Dr. Soumia MERMOUL ENP

Examiner: Dr. Oussama DJEMA CRTSE

Dr. Youssef LARBAH CRNA

Guest: Mr. Omar MENCHI CRND

ENP 2025

REPUBLIQUE ALGERIENNE DEMOCRATIQUE ET POPULAIRE

Ministère de l'Enseignement Supérieur et de la Recherche Scientifique





Département de génie des matériaux

Centre de Recherche Nucléaire de Draria



Mémoire de projet de fin d'études

pour l'obtention du diplôme d'ingénieur d'état en génie des matériaux

Impact d'un dépôt de béryllium sur la fiabilité des soudures Zircaloy-4/Zircaloy-4 pour les crayons combustibles en réacteurs de recherche HMWRR

Presenté par :

TAYSSIR Soundousse Nadjlaa

Sous la direction de:

Pr. LARIBI Merzak ENP

Dr. SAHLI Amane CRND

Présenté et soutenu publiquement le 08 juillet 2025

Membres du jury:

Président: Dr. MERMOUL Soumia ENP

Examinateur: Dr. DJEMA Oussama CRTSE

Dr. LARBAH Youssef CRNA

Invité: M. MENCHI Omar CRND

ENP 2025

ملخص:

يقيّم هذا المشروع أداء البيريليوم كمعدن لحام في عملية ربط المكوّنات الهيكلية المصنوعة من Zircaloy-4 مثل الوسادات والفواصل ضمن تجميعات الوقود النووي. تهدف هذه الدراسة إلى توصيف خصائص الوصلات الملحومة وتحديد العوامل الأساسية التي تؤثر على أدائها ومتانتها تحت الظروف الخاصة بالمفاعلات البحثية. تتضمن عملية التوصيف التجريبي كلاً من المجهر الضوئي، والمجهر الإلكتروني الماسح(SEM)، والتحليل الطيفي بالأشعة السينية المشتتة للطاقة (EDS)، واختبارات الصلادة الدقيقة. تُظهر النتائج أن تحضير السطح يؤثر بشكل حاسم على جودة الوصلة، وأن التحكم الدقيق في كمية البيريليوم المترسبة أمر ضروري، كما تبيّن أن الواجهة متجانسة وأن الوصلات تظهر استقرارًا ميكانيكيًا جيدًا. تؤكد هذه النتائج ملاءمة استخدام البيريليوم في عمليات اللحام مع Zircaloy-4 في ظل ظروف محكمة.

Résumé:

Cette étude évalue les performances du béryllium en tant que métal d'apport pour le brasage des composants structurels en Zircaloy-4 (patins et espaceurs) dans les assemblages de combustible nucléaire. Elle vise à caractériser les propriétés de cette jonction de brasage, et d'identifier les facteurs clés de performance et de durabilité dans les conditions spécifiques des réacteurs de recherche. La caractérisation expérimentale comprend la microscopie optique, la microscopie électronique à balayage (MEB), la spectroscopie à dispersion d'énergie (EDS) et les essais de microdureté. Les résultats démontrent que la préparation de surface influence de manière cruciale la qualité du joint, un contrôle précis du dépôt de béryllium est essentiel, l'interface présente une homogénéité structurale, et les joints présentent une stabilité mécanique. Ces conclusions confirment l'adéquation du brasage au béryllium pour le Zircaloy-4 dans des conditions contrôlées.

Mots-clés: Zircaloy-4, béryllium, brasage, patins et entretoises, jonction de brasage.

Abstract:

This project assesses the performance of beryllium as a brazing metal for joining Zircaloy-4 structural components (pads and spacers) in nuclear fuel assemblies. This study aims to characterize the properties of the brazed joint and identify the key performance and durability factors under the specific conditions of research reactors. Experimental characterization includes optical microscopy, scanning electron microscopy (SEM), energy-dispersive X-ray spectroscopy (EDS), and microhardness testing. The results show that surface preparation critically influences joint quality, precise control of beryllium deposition is essential, the interface is homogeneous, and the joints exhibit mechanical stability. These findings confirm the suitability of beryllium brazing for Zircaloy-4 under controlled conditions.

Key words: zircaloy-4, beryllium, brazing, pads and spacers, brazed joint.

"The results of this work are the property of the Draria Nuclear Research Center. Any partial or complete publication of the results without prior authorization from COMENA will be subject to legal action"

Acknowledgments

First and foremost, I thank Allah, the Almighty, for granting me faith, willpower, and courage to accomplish this humble work.

I would like to express my deepest gratitude to Dr. Amane SAHLI, my supervisor at the Draria Nuclear Research Center (CRND), for her exceptional guidance, generosity, and unwavering support throughout this project. Her expertise, trust, and dedication were instrumental in every stage of this work.

I also wish to thank Dr. Merzak LARIBI, my academic supervisor at the National Polytechnic School (ENP), for his guidance and valuable feedback during the academic preparation of this thesis. I am especially grateful for the time and attention he devoted to reviewing and correcting the manuscript.

I extend my sincere appreciation to Mr. Omar MENCHI and Mr. Mohammed SADOUKI from the research center for their technical assistance and support during the experimental phase. Their professionalism and kindness made a real difference in the success of this work.

I would also like to thank the entire staff of the Welding Laboratory for providing a welcoming and professional research environment.

My sincere thanks go as well to the members of the jury, Mr. DJEMA and Ms. MERMOUL, and Mr. LARBAH for taking the time to evaluate my work and for their valuable comments and suggestions, which helped enrich this thesis.

Finally, I wish to express my heartfelt gratitude to my mother, father, and sister for their constant love, encouragement, and patience. Their presence and unwavering support have been my greatest source of strength throughout this journey.

Dedications

T	1	7	. 1 •	1	
•	doc	licate	thic	111011	to '
1	ueu	ucuie	uus	WUIN	w.

To my parents,

for their endless love, sacrifices, and support throughout this journey especially to my mother, whose strength, patience, and unwavering care carried me through the hardest moments.

To my sister Alaa,

whose joyful spirit and comforting presence have brightened even the most difficult days.

To the memory of my uncle Redouane,

whose loss left a deep void in my life. Your words and belief in me still echo in my heart and continue to inspire me to strive for excellence.

Soundousse.

Table of contents:

List of figure

List of tables

(Gener	al introduction	12
		Chapter 1: Overview of Zirconium Allo	vs
1	Intı	roduction	
2		ysical properties of zirconium:	
3	_	alloys	
	3.1	Zircaloy-2	
	3.2	Zircaloy-4	
4	Мс	orphological Characterization of the Microstructure	
5		luence of alloying elements	
6		plications of Zirconium and Its Alloys	
7		nclusion	
		Chapter 2: Overview of Brazing	
1	Int	roduction	29
2	Pri	nciple of brazing	29
3		azing Mechanisms	
4	Bra	azing Methods	31
5	Ele	ements Influencing Brazing	32
6	Co	nclusion	33
		Chapter 3: Experimental methods	
1	Int	roduction	35
2	Ma	ıterial	35
3	We	elding of pads and spacers	37
	3.1	Cleaning of structural elements	37
	3.2	Beryllium deposits	
	3.3	Attachment of pads and spacers to tubes	
	3.4	Brazing	40

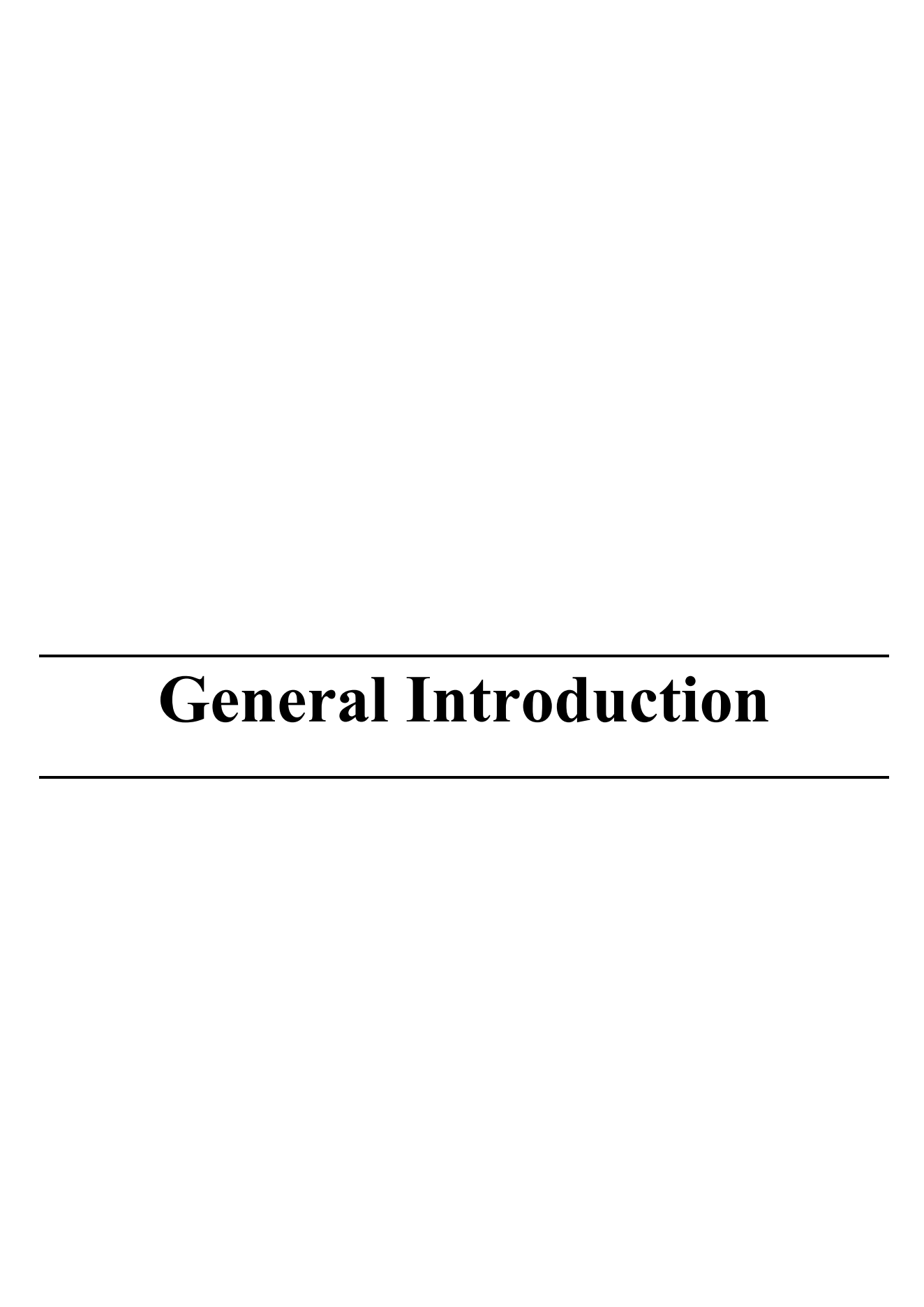
4	Micr	ostructural Characterization:	41
	4.1	Preparing	41
	4.1.1	Cutting	41
	4.1.2	Mounting	41
	4.1.3	Polishing	41
	4.1.4	Chemical etching:	41
	4.2	Optical Microscopy (MO)	41
	4.3	Visual inspection	42
	4.4	X-ray diffraction (XRD) characterization	42
	4.5	Scanning Electron Microscopy (SEM) Characterization	43
5	Mecl	hanical characterization	44
	5.1	Vickers microhardness:	45
6	Conc	clusion	46
		Chapter 4: Results and Discussion	
1	Intro	duction	48
2	Macı	roscopic Characterization	48
3	Micr	ostructural Characterization	49
	3.1	Optical Micrography	49
	3.2	SEM Characterization	53
	3.3	XRD Characterization	58
4	Micr	ohardness Profile	59
5	Conc	clusion	61
G	General	l Conclusion	63
O	utlook	k and Future Work	64
В	ibliogi	raphy	66
A	ppend	lices	69

List of figures

Figure 1.1: Widmanstätten structure	23
Figure 3.1: Pads, spacers, and Zircaloy-4 tube	35
Figure 3.2: Thermo Scientific Niton XRF Analyzer Software Interface	36
Figure 3.3: Shot blasting machine	37
Figure 3.4: Vacuum metallization equipment	38
Figure 3.5: Capacitor discharge welding equipment	39
Figure 3.6: Brazing equipment	40
Figure 3.7: Photo of the Optical Microscope and the lighting device	42
Figure 3.8: PHILIPS X'PERT PRO MPD Powder Diffractometer	43
Figure 3.9: ZEISS Gemini SEM 300 Scanning Electron Microscope	44
Figure 3.10: Semi-automatic microhardness tester on the left and example of a mic imprint on the right	
Figure 4.1: Surface morphology of spacers after sandblasting, without surface trea	
after beryllium deposition	
Figure 4.2: (a) Localized oxidation in the brazing zone, (b) Bonding defect, (c) Ex	
beryllium at the joint	
Figure 4.3: Microstructure of Zircaloy-4 cladding after brazing (<i>Widmanstätten</i> str Figure 4.4: Microstructure of the brazed joint between the pad and the Zircaloy-4 of	
Figure 4.5: Two spacer-cladding brazed joints for two spacers	_
Figure 4.6: Localized porosity at the pad–cladding interface	
Figure 4.7: Welding defect due to non-uniform beryllium deposition	
Figure 4.8: Excess beryllium defect in the brazing zone	
Figure 4.9: SEM microstructure of the Zr–Be brazed joint	
Figure 4.10: EDS chemical mapping of the Zr–Be brazed zone	
Figure 4.11: Elemental concentration profile (line scan) across the Zr–Be brazed z	one 58
Figure 4.12: X-ray diffraction (XRD) spectrum of the brazed Zircaloy-4 sample	59
Figure 4.13: Microhardness profile of the spacer-cladding interface in Zircaloy-4	brazed with
beryllium	60
Figure 4.14: Microhardness profile for double spacers—Zircaloy-4 cladding brazed	with
beryllium	60

List of tables

Table 1.1: main physical properties of zirconium	16
Table 1.2: influence of alloying elements on the phase domains of zircaloy-4	24
Table 3.1: composition in % by mass of the alloy from the zircaloy-4 study	36



General introduction

In the field of nuclear energy, the reliability of fuel assemblies is a fundamental requirement for ensuring reactor safety and performance. The CANDU (Canada Deuterium Uranium) pressurized heavy water reactor uses tubular fuel rods made of zirconium-based alloys, which are known for their low neutron capture cross-section and good resistance to severe operating conditions.

The manufacturing process for CANDU fuel elements is based on the assembly of Zircaloy-4 tubular cladding, to which structural components such as pads and spacers are attached. These components ensure the spacing between the rods and facilitate homogeneous core cooling. Their attachment requires precise processes, such as brazing, to ensure a mechanically robust and stable joint over the long term.

Unlike welding, brazing enables two materials to be joined without melting, thanks to the interposition of a filler metal whose melting point is lower than that of the base materials. In this study, beryllium is used as the brazing metal for the bond between the pads/spacers and the Zircaloy-4 tubes. Beryllium was chosen for its remarkable physicochemical properties: low density, good thermal conductivity and the ability to form strong metallurgical bonds with zirconium. However, the use of beryllium also entails significant health risks: beryllium is a toxic element whose dust can cause serious diseases, such as berylliosis, requiring rigorously controlled handling in a confined environment.

The aim of this work is to study the metallurgical phenomena involved in brazing Zircaloy-4 components, shedding light on beryllium deposition conditions, brazed joint formation mechanisms, and the mechanical and microstructural properties of the assemblies obtained. To meet these objectives, the study is divided into four chapters:

- Chapter 1: General information on zirconium alloys, covering the properties, development and use of zircaloy alloys, particularly in the nuclear industry.
- Chapter 2: Brazing, which describes the basic principles of the process, the physicochemical mechanisms involved, existing methods, and the factors influencing joint quality.

General Introduction

- Chapter 3: Experimental methods, describing in detail the protocol applied for preparation, beryllium deposition and component brazing, as well as the various characterization techniques used (MO, SEM, XRD, microhardness).
- Chapter 4: Results and interpretations, in which the results obtained are analyzed in terms of microstructure, mechanical behavior and weld quality, in order to draw relevant conclusions for industrial optimization of the process.

This work is part of an effort to understand and control joining processes in a highly demanding context, by balancing the technical performance required with the health and industrial constraints inherent in the use of beryllium.

Chapter 1

Overview of Zirconium Alloys

1 Introduction

Zirconium alloys are primarily used for manufacturing cladding tubes that encase nuclear fuel pellets. Their main advantage lies in their extremely low thermal neutron capture cross-section, which helps maintain a favorable neutron economy within the reactor core. In addition to this nuclear benefit, these alloys exhibit excellent dimensional and microstructural stability under prolonged irradiation, ensuring fuel reliability throughout its service life. They also show outstanding corrosion resistance in high-temperature, high-pressure aqueous environments, a critical factor in pressurized water reactors. Furthermore, zirconium alloys possess favorable mechanical properties, including good ductility, high tensile strength, and satisfactory creep behavior, allowing them to withstand the thermomechanical stresses encountered in reactor operation. Ongoing optimization of their chemical composition and microstructure continues to enhance their performance and contribute to the overall safety and efficiency of nuclear reactors [1, 14, 22].

2 Physical properties of zirconium:

Zirconium, due to its extremely low thermal neutron capture cross-section, was quickly recognized as a strategic material for nuclear applications, particularly in reactor core components where minimizing neutron absorption is critical for maintaining efficient chain reactions. In addition to its neutron transparency, zirconium offers a unique combination of high corrosion resistance, good mechanical strength, and thermal stability, making it ideal for use in fuel cladding and structural elements under harsh reactor conditions.

Table 1.1 summarizes the key physical properties of zirconium at room temperature, which contribute to its suitability in high-performance environments such as pressurized water reactors (PWRs) and boiling water reactors (BWRs).

Chapter 1: Overview of Zirconium Alloys

Table 1.1: Main physical properties of zirconium [1, 2, 28]

Property	Value
Density at 20°C (g/cm³)	6.5
Melting point (°C)	1850
Thermal neutron capture cross-section (barns)	0.185
Specific heat at 20°C (J/kg/°C)	276
Thermal diffusivity at 20°C (10 ⁻² cm ² /s)	11.8
Thermal conductivity at 20°C (W/m/°C)	21.1
Electrical resistivity at 20°C (μΩ·cm)	44
Young's modulus at 20°C (MPa)	98,000
Shear modulus at 20°C (MPa)	36,500
Poisson's ratio at 20°C	0.35

These properties make zirconium a material of choice in reactor engineering, where a balance between neutron economy, thermal performance, and structural integrity is essential.

3 Zr alloys

The primary zirconium-based alloys developed and widely used in nuclear reactors can be grouped into three main families, each tailored to meet specific performance requirements in terms of corrosion resistance, mechanical strength, and irradiation behavior [1, 13, 24]:

- Zircaloy-type alloys (notably Zircaloy-2 and Zircaloy-4): These are traditional zirconium alloys primarily alloyed with tin (~1.5%), which enhances mechanical properties and corrosion resistance [1, 21]. They also contain minor additions of iron, chromium, and, in the case of Zircaloy-2, nickel, which help control corrosion and phase stability [3, 24]. Zircaloy-2 is often used in boiling water reactors (BWRs) [1, 14], while Zircaloy-4, with reduced nickel content, is preferred in pressurized water reactors (PWRs) due to its improved resistance to nodular corrosion [21, 25].
- **Zr-Nb-type alloys:** These modern alloys contain **1 to 2.5% niobium**, and in some cases, small amounts of **tin or iron**. Niobium acts as a β-phase stabilizer and significantly improves corrosion resistance under irradiation [13, 24, 26]. Alloys such

as **Zr-1Nb** and **Zr-2.5Nb** are commonly used in pressure tubes and cladding in advanced reactor designs, including CANDU reactors [13, 26].

• Zr-Sn-Fe-Nb-type alloys (e.g., Zirlo, E635): These advanced alloys combine tin, iron, and niobium to balance mechanical performance and corrosion resistance, particularly under high burn-up conditions [24, 26]. Zirlo, widely adopted in PWR fuel cladding, offers superior dimensional stability and irradiation resistance compared to conventional Zircaloys [13, 26]. E635, containing additional chromium and vanadium in some cases, is used in VVER-type reactors for its enhanced strength and creep resistance [24, 26].

3.1 Zircaloy-2

Zircaloy-2 was developed in the early 1950s as one of the first nuclear-grade zirconium alloys, primarily for use in boiling water reactors (BWRs) [1, 3, 24]. Its chemical composition is carefully controlled to balance mechanical strength, corrosion resistance, and neutron economy. The typical composition of Zircaloy-2 is as follows: [1]

- Tin (Sn): 1.2–1.7 wt%
- Iron (Fe): 0.07–0.20 wt%
- Chromium (Cr): 0.05–0.15 wt%
- Nickel (Ni): 0.0 –0.08 wt%
- Oxygen (O): 0.10–0.14 wt%
- Zirconium (Zr): Balance

The inclusion of nickel distinguishes Zircaloy-2 from later alloys and plays a significant role in its corrosion behavior and hydrogen pickup.

Zircaloy-2 consists of an α -zirconium matrix with intermetallic second-phase particles (SPPs) dispersed throughout. Two primary types of intermetallics are present:

• **Zr(Cr,Fe)**² **Laves phase:** These particles are typically 0.1–0.5 µm in size and contribute to corrosion resistance by influencing oxide growth kinetics and acting as cathodic sites during corrosion [2].

• **Zr₂(Ni,Fe) phase:** Nickel-containing intermetallics unique to Zircaloy-2, generally smaller and less stable, have been linked to increased hydrogen pickup and nodular corrosion susceptibility [1, 3, 24, 27].

The distribution and morphology of these precipitates are influenced by heat treatment and thermomechanical processing, which also develop the characteristic crystallographic texture critical for mechanical anisotropy and irradiation behavior.

Zircaloy-2 exhibits mechanical properties suitable for fuel cladding and structural components in BWRs:

- Yield Strength: Typically in the range of 300–400 MPa at room temperature, influenced by tin and oxygen content [1].
- **Ductility:** Good ductility with elongations around 20–30%, allowing the alloy to withstand stresses during reactor operation and handling.
- Fracture Toughness: Zircaloy-2 generally shows lower fracture toughness compared to Zircaloy-4, especially at higher hydrogen concentrations, due to hydride embrittlement associated with its nickel content [3].
- Creep Resistance: Adequate creep resistance at operating temperatures (~280–320°C), with strength enhanced by tin and oxygen solid solution strengthening.

Zircaloy-2 is renowned for its excellent corrosion resistance in BWR environments:

- **Nodular Corrosion Resistance:** Zircaloy-2 resists nodular corrosion, a localized accelerated corrosion form prevalent in BWRs. The presence of nickel and the nature of intermetallic precipitates contribute to this behavior [1].
- **Hydrogen Pickup:** Zircaloy-2 absorbs more hydrogen during corrosion compared to Zircaloy-4, primarily due to nickel content. This hydrogen uptake leads to hydride formation, which embrittles the alloy and can cause delayed hydride cracking [2].
- Oxide Layer: The oxide formed is primarily monoclinic ZrO₂, which acts as a protective barrier but can crack or spall under thermal or mechanical stresses, affecting long-term corrosion resistance.

Chapter 1: Overview of Zirconium Alloys

Corrosion Kinetics: Corrosion proceeds with an initial rapid oxide growth phase

followed by a slower steady-state regime. The oxide thickness and hydrogen pickup

increase with exposure time and temperature.

Under neutron irradiation in reactor cores, Zircaloy-2 undergoes several microstructural and

property changes:

Irradiation Growth: Anisotropic dimensional changes due to defect accumulation

and texture effects cause elongation or contraction, impacting fuel rod geometry [1].

SPP Dissolution: Irradiation can cause partial dissolution or amorphization of

Zr₂(Fe,Ni) precipitates, degrading corrosion resistance and increasing hydrogen pickup

[3].

Hydride Formation and Reorientation: Increased hydrogen uptake leads to hydride

precipitation, which can reorient under stress, reducing fracture toughness and

increasing susceptibility to delayed hydride cracking.

Radiation-Induced Segregation: Alloying elements may segregate at grain

boundaries under irradiation, influencing corrosion and mechanical behavior.

3.2 Zircaloy-4

Zircaloy-4 was introduced as an evolution of Zircaloy-2 to address specific limitations

observed in pressurized water reactors (PWRs), particularly related to hydrogen pickup and

corrosion performance. The critical compositional change was the near elimination of nickel,

which was found to exacerbate hydrogen uptake and nodular corrosion in Zircaloy-2 [1, 21,

27].

Typical composition ranges for Zircaloy-4 are:

Tin (Sn): 1.2 - 1.7 wt%

Iron (Fe): 0.18 - 0.24 wt%

Chromium (Cr): 0.07 - 0.13 wt%

Nickel (Ni): <0.01 wt% (effectively removed)

Oxygen (O): 0.10 - 0.14 wt%

Zirconium (Zr): Balance

19

Chapter 1: Overview of Zirconium Alloys

The increase in iron content compensates for the removal of nickel, maintaining corrosion resistance and mechanical strength. The alloying elements are carefully balanced to optimize phase stability, microstructure, and neutron economy [2].

Zircaloy-4 is typically produced by melting and casting followed by hot extrusion and cold pilgering to form tubing. Subsequent heat treatments, including annealing below the β -transus temperature (~865°C), refine grain size and develop the characteristic crystallographic texture essential for in-service performance [1].

The alloy's microstructure consists of an α-zirconium matrix with finely dispersed Zr(Cr,Fe)₂ intermetallic particles. The absence of nickel eliminates the formation of Zr₂(Ni,Fe) precipitates, resulting in a more stable and homogeneous microstructure under irradiation

The microstructure of Zircaloy-4 is dominated by equiaxed or elongated α -phase grains, depending on processing history. The intermetallic Zr(Cr,Fe)₂ particles are typically 0.1–0.5 μ m in size and distributed along grain boundaries and within grains [1].

The cold pilgering and annealing processes induce a strong basal texture, with basal poles oriented approximately 30° from the tube radial direction. This texture influences:

- **Mechanical Anisotropy:** Yield strength and ductility vary with loading direction due to the hcp crystal symmetry.
- Irradiation Growth: Anisotropic dimensional changes under neutron irradiation are texture-dependent.
- **Hydride Orientation:** Hydrides preferentially precipitate on basal planes, affecting embrittlement and fracture behavior [2].

Annealing treatments control grain size, typically targeting 5–15 µm for optimal balance between strength and corrosion resistance. Fine grains improve strength but may increase corrosion susceptibility, while coarse grains enhance corrosion resistance but reduce strength [1].

Zircaloy-4's mechanical properties are tailored for the demanding environment inside PWR cores:

• Yield and Tensile Strength: Typically, 350–450 MPa at room temperature, influenced by tin and oxygen solid solution strengthening and precipitation hardening from SPPs.

- **Ductility:** Maintains elongations of 20–30%, essential for accommodating thermal and mechanical strains during operation.
- **Fracture Toughness:** Superior to Zircaloy-2, especially at elevated hydrogen concentrations. The absence of nickel reduces hydride embrittlement, improving crack resistance [3].
- Creep and Fatigue Resistance: Adequate creep strength at operating temperatures (~300°C) and good fatigue resistance support long fuel cycles and reactor safety.

Zircaloy-4 exhibits excellent corrosion resistance in PWR environments due to its optimized composition and microstructure:

- Oxide Layer Characteristics: Forms a dense, adherent monoclinic ZrO₂ oxide layer that protects the substrate metal. The oxide grows slowly after an initial rapid phase, following parabolic kinetics [1].
- **Hydrogen Pickup:** Significantly reduced compared to Zircaloy-2, leading to lower hydride formation and improved ductility retention over extended service [2].
- Corrosion Mechanisms: The corrosion process involves oxidation of zirconium at the metal/oxide interface, oxygen diffusion through the oxide, and hydrogen generation. The alloying elements influence oxide growth rate, protect against localized corrosion, and affect hydrogen diffusion [1].
- Effect of Irradiation: Irradiation enhances corrosion rates and hydrogen pickup but Zircaloy-4's stable microstructure mitigates these effects better than Zircaloy-2 [3].

Zircaloy-4 demonstrates improved irradiation performance compared to Zircaloy-2:

- **Dimensional Stability:** Texture and microstructure reduce irradiation growth and creep deformation, maintaining fuel rod geometry [1].
- SPP Stability: Zr(Cr,Fe)₂ precipitates remain stable under neutron flux, preserving corrosion resistance and mechanical integrity.
- **Hydride Behavior:** Lower hydrogen pickup reduces hydride precipitation and associated embrittlement risks.

Radiation-Induced Segregation: Less pronounced in Zircaloy-4, leading to better grain boundary stability and corrosion resistance [2].

4 Morphological Characterization of the Microstructure

The microstructure resulting from the $\beta \rightarrow \alpha$ transformation in zirconium alloys is highly dependent on the cooling rate [1,13,23]. A martensitic structure, consisting of very fine needle-like plates, forms when the cooling rate exceeds 2000 K/s [23,29]. At slower cooling rates, particularly below 200 K/s, all observations show the formation of a lamellar microstructure known as Widmanstätten structure (Figure 1.1) [1,13].

This Widmanstätten structure typically appears in two main forms [1,13,23]. The first, known as the "basket-weave" structure, consists of short, entangled lamellae that appear to have nucleated randomly within the prior β -grain [13,23]. The second, called the "parallel platelets" structure, is characterized by long, parallel lamellae that form alpha-phase grain colonies [1,23]. These colonies appear to nucleate and grow from the prior β -grain boundaries [1,13,23].

Several factors influence the development of one form over the other [13,23]. Insoluble particles in the β -phase, such as ZrC carbides, Zr₃Si silicides, or ZrP phosphides, can act as nucleation sites [1,23]. Their heterogeneous distribution within the former β -grain results in varying microstructures [13,23]. Notably, β -grain boundaries also serve as preferential nucleation sites [1,13]. When nucleation occurs primarily within the grain volume—typically promoted by large prior β -grains or high cooling rates—a basket-weave structure tends to form [13,23]. In contrast, preferential nucleation at grain boundaries—encouraged by smaller β -grain sizes or slower cooling rates—leads to a parallel platelet structure [1,13].

The effect of cooling rate on microstructure can be explained as follows [1,23]: under slow cooling, lamellae grow from prior β -grain boundaries where nucleation is energetically favorable [13,23]. Simultaneously, the thickness of the lamellae increases due to the longer diffusion time of alpha-stabilizing elements [1,29]. On the other hand, under rapid cooling, nucleation on nano-precipitates distributed within the prior β -grain becomes energetically favorable [23,29]. Due to the short diffusion time of alpha-stabilizing elements in such conditions, the growth of lamellar thickness is limited [1,23,29].

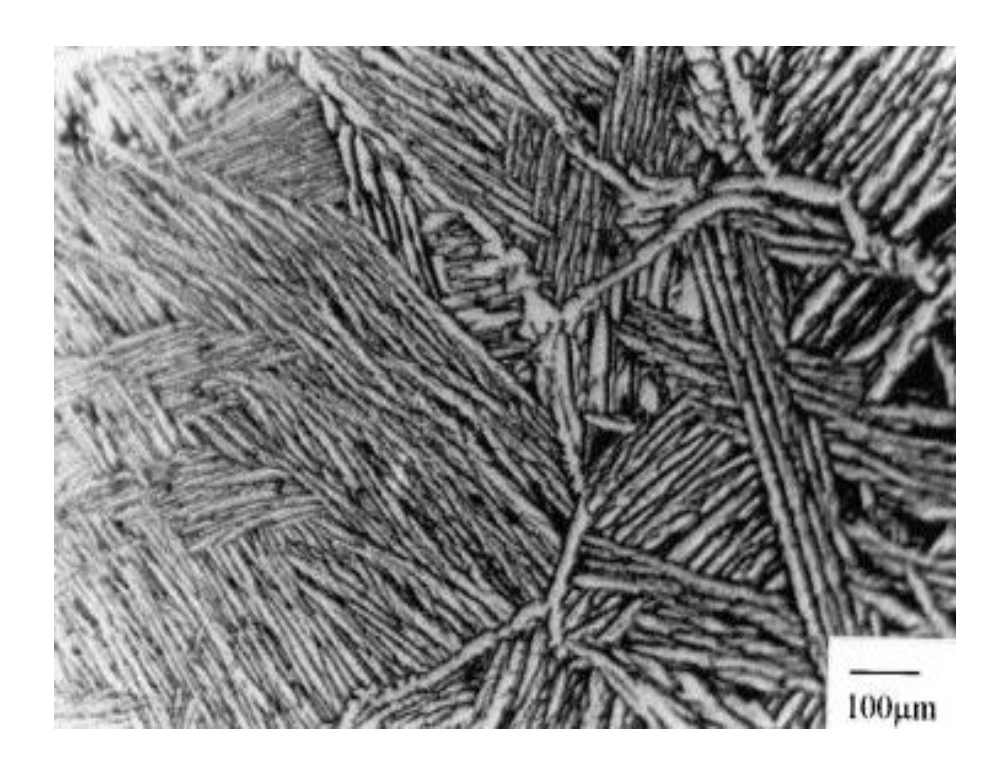


Figure 1.1: Widmanstätten structure

5 Influence of alloying elements

The alloying elements present in Zircaloy-4 (Zry-4) create a biphasic domain composed of hexagonal close-packed (hcp, or α -phase) and body-centered cubic (bcc, or β -phase) structures between approximately 810 °C and 980 °C [1, 13, 23]. These alloying elements play a critical role in modifying the phase stability and transformation behavior of zirconium [1, 24].

They can generally be classified into two categories: alpha (α) stabilizers, which promote the stability of the α -phase and elevate the allotropic transformation temperature [1, 21], and beta (β) stabilizers, which instead favor the β -phase and reduce the temperature at which the $\alpha \rightarrow \beta$ phase transformation occurs [1, 13, 26].

Among the β stabilizers, a specific subgroup known as eutectoid beta stabilizers—including elements such as Fe, Cr, Ni, Cu, Si, Nb, and V—induces a eutectoid decomposition of the β -phase when combined with zirconium [1, 13, 24]. These elements exhibit high solubility in the β -phase at elevated temperatures but have limited solubility in the α -phase. As the material cools, they tend to precipitate from the α -phase as finely dispersed intermetallic compounds, which can significantly influence the mechanical properties, corrosion resistance, and microstructural stability of the alloy.

Table 1.2: Influence of Alloying Elements on the Phase Domains of Zircaloy-4

		Influence on the phase diagram	Elements
Alpha stabilizers	S	865°C α + β	O, Sn, Al, N, Hf
	Isomorphous elements	T	Ti
Beta stabilizers	Eutectoid elements	T 865°C α α+Z _r χ	Fe, Cr, Ni, Nb, Cu, V.

- Oxygen (O) is to be considered as an alloying element and not an impurity it has a high solubility in the alpha phase and stabilizes at high temperatures [1,21]. Oxygen is added to increase the yield strength through solution strengthening by occupying the octahedral interstitial sites in the crystal lattice, without degradation of corrosion resistance [1,21,25]. Typical concentrations range from 800 to 1600 ppm exceeding 1500 ppm of oxygen can reduce ductility [21,24]. In addition, Oxygen interacts with dislocations at moderate temperatures, leading to age-strengthening phenomena that depend on strain rate [13,23]. In the Zr-O system, the only stable oxide is ZrO₂ with a

- monoclinic structure stable up to about 1200 °C, above which it transforms into a tetragonal phase [1,18].
- Tin (Sn) tends to expand the α-phase domain in zirconium, and its maximum solubility in the hexagonal close-packed (hcp) zirconium is about 9 wt% at 940°C [1]. Originally, Sn was added at concentrations between 1.2% and 1.7% to improve corrosion resistance, especially by mitigating the harmful effects of nitrogen (N) [21,24]. For example, to compensate for 300 ppm of nitrogen in zirconium, approximately 1% of Sn is needed [21]. However, in nitrogen-free zirconium, it has been observed that Sn can actually deteriorate corrosion resistance [21]. Therefore, the current trend is to slightly reduce the amount of Sn to maintain good creep properties and overall performance, without significantly compromising corrosion resistance [24,26].
- **Iron, chromium**, and **nickel**, at their typical concentrations, are completely soluble in the β-phase [1]. However, their solubility in the α-phase is very limited, approximately 120 ppm for Fe and 200 ppm for Cr at their maximum solubility temperature [1,23]. In pure binary systems, different intermetallic phases can form: ZrFe₂ and ZrCr₂ are Laves phases with either cubic or hexagonal crystal structures, while Zr₂Ni is a Zintl phase with a body-centered tetragonal (C16) structure [1,24]. These precipitates are called the Second Phase Particles (SPPs). In commercial Zircaloys, iron substitutes for other transition metals, resulting in the formation of Zr₂(Ni,Fe) and Zr(Cr,Fe)₂ intermetallic compounds [13,24]. The specific composition and structure of these SPPs significantly influence the alloy's mechanical properties [13,27] and corrosion resistance [21,24].
- Niobium (Nb) is a strong β-phase stabilizer used primarily in advanced zirconium alloys such as ZIRLO and M5 [13,26]. It lowers the α↔β transformation temperature [1,26] and contributes to improve corrosion resistance and mechanical strength, especially under irradiation [24,26]. Although its solubility in the α-phase is limited, Nb can form fine, stable precipitates that help refine the microstructure and enhance performance in pressurized water reactors [23,26]. Due to its low neutron absorption and favorable in-reactor behavior, niobium is a preferred alloying element in modern nuclear cladding materials [24,26].

- **Sulfur** has recently been found to be highly effective in enhancing creep resistance, even at very low concentrations of 30-50 ppm [13,24]. Previously not regarded as significant, sulfur is now intentionally added during processing to reduce variability in mechanical behavior and to improve high-temperature strength [13,24].

The effectiveness of such low levels of sulfur on creep properties is attributed to the segregation of sulfur atoms at dislocation cores, which alters their core structure [23,24]. Importantly, sulfur does not impact the corrosion properties of the alloy.

6 Applications of Zirconium and Its Alloys

Zirconium and its alloys are widely used across various high-performance industries due to their unique combination of properties such as excellent corrosion resistance, high melting point, good mechanical strength, and low neutron absorption cross-section [1,14,22]. The main application domains include:

- Nuclear Industry: Zirconium alloys (such as Zircaloy-2, Zircaloy-4, and Zr-Nb systems) are extensively used in nuclear reactors, particularly for fuel cladding and structural components in both pressurized water reactors (PWRs) and boiling water reactors (BWRs) [1,14,24]. Their low neutron absorption makes them ideal for maintaining efficient nuclear reactions while withstanding extreme environments [1,22,26].
- Chemical and Petrochemical Industries: Thanks to their outstanding resistance to corrosive agents such as acids, alkalis, and organic solvents, zirconium alloys are used in heat exchangers, reactors, piping systems, and valves in chemical processing plants [1,17,21].
- Aerospace and Defense: Zirconium's strength-to-weight ratio and thermal stability make it suitable for aerospace components exposed to high temperatures or corrosive environments [1,26]. It's also used in certain defense applications, including missile and propulsion systems [17,22].
- **Medical Field**: Biocompatible grades of zirconium are used in surgical implants, dental devices, and prosthetics due to their non-toxic and corrosion-resistant nature in biological environments [1,17,25].

• Electronics and Specialty Applications: Zirconium is employed in the production of capacitors, vacuum tubes, and as a getter in electronic devices due to its ability to absorb residual gases [1,17]. In addition, its compounds (e.g., zirconia) are used in oxygen sensors, fuel cells, and advanced ceramics [1,18,22].

7 Conclusion

Zirconium alloys exhibit two phases: the α -phase, with a hexagonal close-packed (HCP) structure, which is stable at low temperatures, and the β -phase, with a body-centered cubic (BCC) structure, which becomes stable above the transus temperature—around 865 °C for pure zirconium.

Alloying elements influence both the extent of the two-phase $(\alpha + \beta)$ region and the kinetics of phase transformation. Depending on the quenching rate, the resulting α -phase structures can vary.

During the manufacturing processes of these alloys, this allotropic transformation is often repeated multiple times. Therefore, studying the resulting microstructure is crucial to better control the subsequent fabrication steps.

The $\beta \rightarrow \alpha$ transformation typically produces a lamellar microstructure known as the Widmanstätten structure, which appears in two main morphologies: basket-weave lamellae and parallel platelet lamellae. These lamellae nucleate within prior equiaxed β -grains, whose crystallographic orientation influences that of the resulting α -grains.

Chapter 2

Overview of Brazing

1 Introduction

Brazing is a widely used metal-joining technique in various industrial applications, particularly when dealing with materials or components that are difficult to weld. Unlike welding, which involves melting the base metals, brazing joins parts by melting a filler metal that flows into the joint via capillary action without melting the base materials. This process allows for the creation of strong, leak-tight, and precise joints, making it particularly suitable for assemblies with complex geometries, thin-walled sections, or dissimilar metals.

The quality and reliability of brazed joints depend on several factors, including the choice of filler metal, joint design, base material compatibility, and the brazing method employed. Understanding the underlying physical and chemical mechanisms—such as wetting, diffusion, and capillary action—is essential for optimizing the brazing process. This document provides an overview of brazing principles, mechanisms, various brazing methods, and the critical factors influencing joint integrity. It aims to serve as a technical reference for researchers, engineers, and practitioners involved in metal joining processes.

2 Principle of brazing

Brazing is a metal-joining process in which a filler metal with a lower melting point than the base metals is used to bond the parts without melting the main components. Unlike welding, where the base metals are melted, brazing involves melting only the filler metal to create a strong metallurgical bond. The process typically occurs above 450°C, and precise fitting of the workpieces is essential to enable capillary action, which draws the filler metal into the joint, ensuring a good bond. The brazing temperature is usually about 50°C higher than the filler metal's melting point for optimal wetting and coverage [4].

Components that are difficult or impossible to join using other methods can often be successfully joined through brazing. It is well suited for making complex assemblies with odd shapes and varying thickness. During the joining process, maintaining tight tolerances is crucial if the joint gap is too wide, capillary action will not effectively draw the braze filler metal (BFM) into the joint. Another problem with brazing is that the brazed joint is not homogenous, the boundary zone has different chemical and mechanical properties compared the base metal. In some cases, certain BFMs can cause the joint to become more prone to corrosion or brittleness [4].

3 Brazing Mechanisms

Several physical and chemical phenomena are central to brazing:

- Capillary Action: Capillary action is the natural ability of a liquid to flow into narrow spaces without assistance, driven by surface tension and adhesive forces between the liquid and solid surfaces. In brazing, this phenomenon is essential for ensuring that the molten filler metal spreads evenly into the joint gap, forming a strong bond upon cooling. The effectiveness of capillary flow depends on proper joint design, including the spacing of the surfaces, and is influenced by factors such as viscosity, vapor pressure, gravity, and metallurgical reactions between the filler metal and base materials. Controlling these factors ensures optimal flow of the filler metal and a high-quality brazed joint [4,5].
- Wetting: Wetting is essential for filler metal adhesion. It occurs when the adhesive forces between the molten filler and the solid base metal exceed the cohesive forces within the liquid. Good wetting ensures the filler metal spreads over and bonds to the surface. Oxide layers or any surface contamination can prevent wetting, so it's really important to keep the joint surfaces clean to ensure a strong, reliable bond [4,5].
- **Diffusion**: At brazing temperatures, atoms of the filler metal diffuse into the base metal, forming metallurgical bonds. While diffusion strengthens the joint, excessive diffusion can cause brittle intermetallic phases or embrittlement, so heat input must be controlled [5,20].
- Metallurgical Reactions: Alloying, carbide precipitation, stress cracking, and embrittlement by elements like hydrogen or sulfur can occur depending on the materials and thermal cycle. These reactions influence joint strength and durability and must be managed carefully [5,21].

4 Brazing Methods

Brazing can be performed using various heating techniques, each suited to specific applications, geometries, and production volumes. The choice of method affects not only the efficiency and precision of the process, but also the quality of the resulting joint.

- Torch Brazing: is a traditional and flexible method where a flame is applied directly to the joint, the flame is generated by the combustion of a combination of oxygen and a fuel gas. It is suitable for low-volume work, repair operations, or when manual control is necessary. The filler metal is introduced when the required temperature is reached, and heating can be easily adjusted by the operator [4,5].
- **Furnace Brazing**: provides uniform heating by placing components in a furnace, usually under a protective atmosphere or in vacuum. It allows for the simultaneous brazing of multiple joints and is ideal for industrial-scale production. The heat is applied evenly to the entire part, reducing thermal distortion and oxidation [4,5,12].
- Induction Brazing: is one of the most advanced and precise heating methods used in modern metal joining. It works by generating eddy currents in conductive materials through a rapidly alternating magnetic field, which directly produces heat within the metal. This technique offers several key advantages:
- **Highly localized and controlled heating**: Only the joint area is heated, which protects nearby components from thermal damage—an essential feature in fields like aerospace and electronics [5,12].
- **Fast and energy-efficient:** Since energy is delivered directly into the material, induction brazing significantly reduces heating times and energy losses, making it up to 80% faster than traditional methods [5,12].
- Exceptional temperature control: With real-time pyrometric monitoring, temperatures can be maintained within a ±2°C range, ideal for sensitive alloys or complex thermal cycles [5].
- Clean, protective atmosphere: Without open flames or combustion gases, induction brazing allows the use of inert or reducing atmospheres (like argon or hydrogen),

Chapter 2: Overview of Brazing

which is critical when working with reactive or oxidation-prone metals such as titanium or stainless steel [5,12].

- **Infrared Brazing**: uses radiant heat from high-intensity quartz lamps, offering precise control over heating time and location [4,5].
- **Dip Brazing**: involves immersing assemblies in a molten salt or filler bath. This ensures uniform heating and is beneficial for complex parts with multiple joints [5].
- **Resistance Brazing:** an electric current is passed through the joint, generating heat by electrical resistance. The filler metal melts and flows into the joint [4,5].

5 Elements Influencing Brazing

Successful brazing depends on the careful consideration of several factors:

- **Base Metal Characteristics**: Properties like strength, thermal expansion coefficient (CTE), and surface condition affect joint quality and residual stress [4, 5].
- Filler Metal Characteristics: The filler must have suitable melting behavior, compatibility with the base metal, and appropriate mechanical and chemical properties including ductility, corrosion resistance, and fatigue strength. Filler metal selection must consider operating conditions and CTE compatibility [4, 5].
- **Joint Design and Clearance**: The shape of the joint (butt, lap, scarf) and the gap size greatly influence the capillary flow and final joint strength. Very small gaps favor strong, void-free joints [4, 5].
- Surface Preparation: Proper cleaning is critical. Surfaces must be free of oxides, grease, and contaminants that inhibit wetting. Cleaning methods include chemical (alkaline cleaning, solvent degreasing, acid pickling) and mechanical cleaning. Brazing should be performed promptly after cleaning to prevent re-oxidation [4, 5].

6 Conclusion

Brazing is a widely used metal-joining technique, especially when the parts to be assembled are complex or made from materials that are difficult to weld. Unlike welding, it relies on a filler metal that melts and flows into the joint by capillary action, without melting the base materials.

The quality of a brazed joint depends on several factors: material selection, joint design, surface condition, heating method, and understanding of physical phenomena such as wetting and diffusion. Various brazing methods exist such as torch brazing, induction brazing, or vacuum brazing each suited to specific production needs.

Chapter 3

Experimental Methods

1 Introduction

As part of this study, a rigorous experimental methodology was implemented to characterize the properties of the materials and evaluate the quality of the assemblies produced. This chapter presents the different stages of the process, from sample preparation to the characterization techniques used. The methods implemented include cleaning and depositing beryllium, fixing and brazing pads and spacers, as well as various microstructural, mechanical, and chemical analysis techniques. Each step has been carefully chosen to ensure reliable and representative results under the actual conditions of use in the nuclear field.

2 Material

Zircaloy-4 is used in the form of tubes (outer diameter: 13.4 ± 0.3 mm; inner diameter: 12.3 mm) for claddings, and strips for pads and spacers with a thickness of 1.1 mm (Figure 3.1).







Figure 3.1: Pads, spacers, and Zircaloy-4 tube

In order to verify the chemical composition of the alloy used in our study, we performed elemental analysis using the Thermo Scientific Niton XRF Analyzer, a portable analyzer based on X-ray fluorescence (Figure 3.2). This non-destructive technique allows rapid and accurate identification of the elements present in the material. The results obtained are presented in the table below and compared to the data provided by the supplier's certificate, in accordance with ASTM B353 – Grade R60804 (Zircaloy-4).



Figure 3.2: Thermo Scientific Niton XRF Analyzer Software Interface

Table 3.1: Composition in % by mass of the alloy from the Zircaloy-4 study

Elements %	Sn	Fe	Cr	V	Zr	О	Н	С	N	HF
ASTM	1.2 – 1.7	0.19 - 0.24	0.07- 0.13	/	97.91	0-16	005	027	025	0 02
Thermo Scientific Niton XRF	1.54	0.142	0,231	0.228	97.79	0	0	0	0	0

- A chromium concentration of 0.231% was found, exceeding the maximum limit defined by ASTM B353, which is 0.13%. This abnormally high value could be explained by local heterogeneity in the material or by the limits of precision related to the XRF analysis method used.
- On the other hand, the presence of vanadium, measured at about 0.228% by mass, is also a notable anomaly, as this element is not part of the usual composition of Zircaloy-4. This detection could reveal either accidental contamination or variation between different batches of raw materials.

3 Welding of pads and spacers

3.1 Cleaning of structural elements

Before being used, the pads, spacers, and tubes are cleaned with water, followed by rinsing with demineralized water. Then, an ultrasonic treatment removes the last traces of impurities.

Only the caps undergo a specific chemical treatment: they are stripped using a mixture of nitric acid, hydrofluoric acid, and water, to properly prepare their surface.

In addition, mechanical stripping is carried out on the active area of the pads and spacers, i.e., the part in direct contact with the tube. This step uses a shot blasting machine that projects abrasive particles to create controlled surface roughness. This texture is essential to ensure good adhesion of beryllium during deposition.

This thorough preparation phase is crucial to ensure a high-quality final coating. It ensures better resistance under service conditions and perfect compatibility with the requirements of the reactor.

The entire process takes place in a controlled environment to avoid cross-contamination and to meet the strict cleanliness standards required in the nuclear field.



Figure 3.3: Shot blasting machine

3.2 Beryllium deposition

Beryllium is deposited on one of the surfaces of the pads and spacers using specialized metallization equipment. This process is carried out inside a vacuum bell designed to accommodate the pad holders and spacer holders, as well as the entire heating system, including the resistors and electrodes.

The process begins by heating the crucible containing the beryllium using electrical resistance until it reaches its boiling point. At this temperature, the beryllium evaporates and turns into metal vapor. Under high vacuum conditions about 10^{-5} mbar, corresponding to a secondary vacuum, these vapors move freely inside the bell. As they condense, they are deposited uniformly on all the metal surfaces present in the bell, particularly the pad holders, the spacer holders, and especially the active surfaces of the pads and spacers themselves.

This deposition process, called PVD (Physical Vapor Deposition), produces a homogeneous and strongly adherent coating, which is essential for withstanding the mechanical and thermal stresses imposed by operating conditions in a nuclear environment.

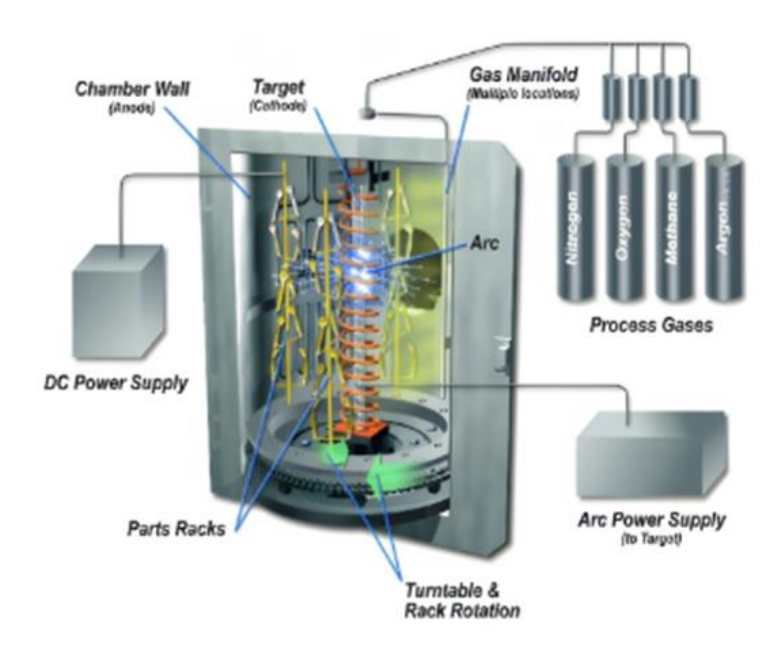


Figure 3.4: Vacuum Metallization Equipment

3.3 Attachment of pads and spacers to tubes

This operation is carried out using equipment called "capacitor discharge". The tube is installed on a specially designed tube holder, which allows it to be held in position throughout the procedure.

At the locations provided for the pads and spacers, suitable masks are placed, into which the components to be treated (pads or spacers) are inserted. The equipment table moves lengthwise in a precise manner, guided by markers and positioning stops. Centering fingers ensure the correct alignment of the pads and spacers at the time of treatment.

A rotating drum also makes it possible to adjust the angular position according to the type of fuel rod processed. Each pencil model has specific geometric characteristics, and the system makes it possible to precisely adapt the position of each element according to these requirements.

The entire device ensures high repeatability and perfect accuracy, which are essential to ensure the quality and reliability of the capacitive discharge treatment process.



Figure 3.5: Capacitor Discharge Welding Equipment

3.4 Brazing

Once the pads and spacers are properly attached to the tube, we proceed to the final step: welding. This operation is carried out using high-frequency brazing equipment, specially designed to heat only the targeted areas, i.e. the three contact points where the pads and spacers are located, without affecting the rest of the tube.

The principle is based on localized heating, which causes the melting of the thin layer of beryllium deposited beforehand. Upon melting, this layer perfectly wets the contact surface between the pad (or spacer) and the tube. This wetting enables metallurgical interaction between beryllium and the tube material, Zircaloy-4 (Zry-4). As a result, beryllium diffuses into the Zry-4, leading to the formation of a Zr-Be eutectic.

This metallurgical phenomenon ensures a strong bond between the two parts: the pad (or spacer) and the tube, thus guaranteeing a durable and high-quality joint, perfectly adapted to the constraints of the nuclear environment.



Figure 3.6: brazing equipment

4 Microstructural Characterization:

4.1 Preparing

4.1.1 Cutting

Axial sections were made using a micro-slicer equipped with a diamond blade, on all TIG welded samples. This step prepares the samples for metallographic analysis.

4.1.2 Mounting

Cold mounting was preferred to prepare the samples for optical microscope analysis. A resin was mixed with a hardener, and then the resulting solution was poured into molds containing the samples.

For samples intended for scanning electron microscopy (SEM), the analysis was carried out without mounting, due to the absence of conductive resin necessary for this type of observation.

4.1.3 Polishing

The mounted samples were mechanically polished to obtain a flat, scratch-free surface suitable for observation under an optical microscope.

The polishing started with the use of abrasive papers with decreasing grain sizes (180, 240, 400, 600, 1000, 1200 up to 4000). Then, a finishing polishing was carried out using a felt fabric and diamond pastes with a grain size of 3 μ m and then 1 μ m, making it possible to obtain a mirror surface suitable for chemical etching and microscopic observation.

4.1.4 Chemical etching:

Prior to optical microscope observation, the mounted samples were subjected to chemical etching to reveal the microstructure of the material. The solution used for this step is composed of 3% hydrofluoric acid (HF), 47% nitric acid (HNO₃) and 50% distilled water. This solution makes it possible to bring out the metallographic contrasts.

Optical Microscopy (MO)All micrographs and macrographs were acquired using a Carl Zeiss optical microscope, model Axio Tech 100. This device is connected to a computer equipped with acquisition software, allowing both the transfer and processing of the obtained images.

4.2 Optical Microscopy (MO)

All micrographs and macrographs were acquired using a Carl Zeiss optical microscope, model Axio Tech 100. This device is connected to a computer equipped with acquisition software, allowing both the transfer and processing of the obtained images.



Figure 3.7: Photo of the Optical Microscope and the lighting device

4.3 Visual inspection

Visual inspection was an essential first step in assessing the quality of the welds. It allowed for examination of the general appearance of the brazed areas in order to detect any defects visible to the naked eye. This step helped identify unwelded areas, discontinuities, or a possible excess of beryllium on the surfaces. Thanks to this simple but effective method, it was possible to perform an initial sorting of the assemblies and to target the samples requiring further examination.

4.4 X-ray diffraction (XRD) characterization

X-ray diffraction provides both qualitative and quantitative information essential for identifying the different phases present in TIG-welded Zircaloy-4. This technique also provides data on crystal structures, lattice parameters, crystallite size, and dislocation density.

X-ray diffraction analyses were performed using a PHILIPS X'PERT PRO MPD "Multipurpose Powder Diffraction" diffractometer (Figure 3.8), equipped with a Bragg-Brentano goniometer operating in $(\theta - \theta)$ mode with a 240 mm radius and a standard resolution of 0.01°. The diffractometer is fitted with a copper source emitting X-rays at a

 $\text{CuK}\alpha$ wavelength of 1.540598 Å, with an acceleration voltage of 30 kV and a current of 40 mA.

All diffraction spectra were recorded over an angular range (2 θ) from 20° to 100°, with an increment of 0.02° and an acquisition time of 350 seconds for each increment.



Figure 3.8: PHILIPS X'PERT PRO MPD Powder Diffractometer

The identification of the different phases is carried out by comparing the sample analyzed with the entries of the PFD-4 (Powder Diffraction File) database version 2018 of the American organization ICDD (International Centre for Data Diffraction) implemented in the X'PertHighScore Plus software of PANalytical.

4.5 Scanning Electron Microscopy (SEM) Characterization

The microstructural examination, as well as the physicochemical analysis of the sample surfaces was carried out using a ZEISS Gemini SEM 300 scanning electron microscope (SEM), illustrated in Figure 3.9. This equipment is coupled to an energy-dispersive X-ray spectroscopy (EDS) microanalysis system, enabling the identification of the elemental composition of the analyzed areas.



Figure 3.9: ZEISS Gemini SEM 300 Scanning Electron Microscope

In addition to classic point analysis, two complementary techniques were used to enhance the interpretation of the results: line scanning, which allows monitoring the variation in concentration of one or more elements along a defined profile, and chemical mapping (elemental mapping), which provides a spatial visualization of the distribution of elements over a given area. These tools make it possible to correlate the micrographic structure more closely with local metallurgical phenomena, for example by identifying areas of diffusion, segregation or intermetallic phase formation.

5 Mechanical characterization

Mechanical characterization allows the evaluation of the key properties of a material under stress, such as its strength or hardness, essential criteria in demanding sectors such as nuclear or aeronautics. Among the available methods, the hardness test is particularly suitable for locally analyzing the resistance to plastic deformation. In this study, only Vickers microhardness was used, due to its accuracy and ability to characterize fine and heterogeneous metallurgical structures.

5.1 Vickers microhardness:

Hardness testing is one of the most commonly used methods for evaluating the mechanical properties of a material, particularly its resistance to localized plastic deformation. It provides precise information on the behavior of the material under concentrated stress.

As part of this study, microhardness measurements were carried out in the mechanical testing and welding laboratory of the Draria Nuclear Research Centre. The tests were carried out using a Vickers microhardness tester, model MHT-10 from the Paar Physica brand, known for its precision and reliability.

The principle of the test is based on the use of a square-based pyramidal diamond indenter. This indenter is applied to the surface of the sample using a specific load. Under the effect of this load, a square imprint is left on the material. The Vickers hardness (denoted HV) is then calculated by dividing the load applied to the surface of the impression, according to the following relationship:

$$HV = F / S$$

where **F** is the applied force (in newtons N) and **S** is the area of the impression (in square millimeters mm²). This method allows a fine characterization of the local resistance of the material, especially in the case of welded or coated metal structures.

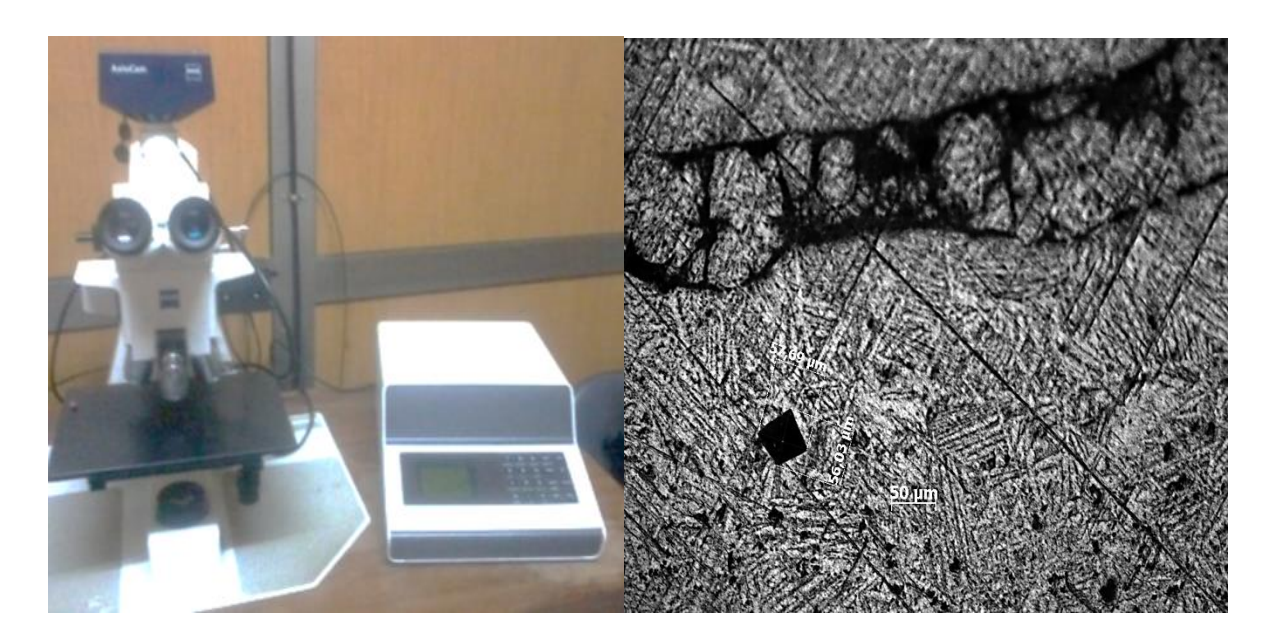


Figure 3.10: Semi-automatic microhardness tester on the left and Example of a Microhardness imprint on the right

6 Conclusion

The various experimental methods detailed in this chapter have enabled the implementation of a complete and structured protocol for the analysis of Zircaloy-4 tubular assemblies. Material control, deposition and welding processes, as well as microstructural and mechanical characterization techniques, have provided a thorough understanding of weld quality and associated metallurgical phenomena. These investigations are essential to validate the conformity of components to the requirements of the nuclear sector, while providing essential technical elements for the optimization of industrial processes.

Chapter 4

Results and Discussion

1 Introduction

As part of the ongoing optimization of fuel assemblies for nuclear reactors, improving the bonding between metallic components represents a critical challenge. This study focuses on the brazing process involving a spacer, a pad, and a Zircaloy-4 cladding using beryllium (99.9% purity) as the filler metal. Particular attention was given to surface preparation, the quality of the metallurgical interface, and the distribution of alloying elements after brazing.

To achieve these objectives, several characterization techniques were employed, including macro- and micrographic observations, scanning electron microscopy with energy-dispersive X-ray spectroscopy (SEM/EDS), X-ray diffraction (XRD), and microhardness measurements. The aim is to gain a deeper understanding of diffusion and interfacial interaction mechanisms in order to evaluate the stability and performance of the resulting joints under conditions similar to those encountered in a nuclear environment.

2 Macroscopic Characterization

Macroscopic examination of the brazed samples allowed for the assessment of the influence of beryllium deposition and surface treatments on the quality of the metallurgical joint. Figure 4.1 illustrates three different configurations: a spacer without beryllium deposition, a spacer with a beryllium layer, and a spacer that underwent sandblasting. This comparison clearly demonstrates the beneficial effect of sandblasting on the surface condition of Zircaloy-4 pads and spacers, as it enhances both surface reactivity and adhesion.

Thus, careful surface preparation is essential to promote uniform diffusion of the brazing material across the interface and ensure the formation of a high-quality, durable joint.

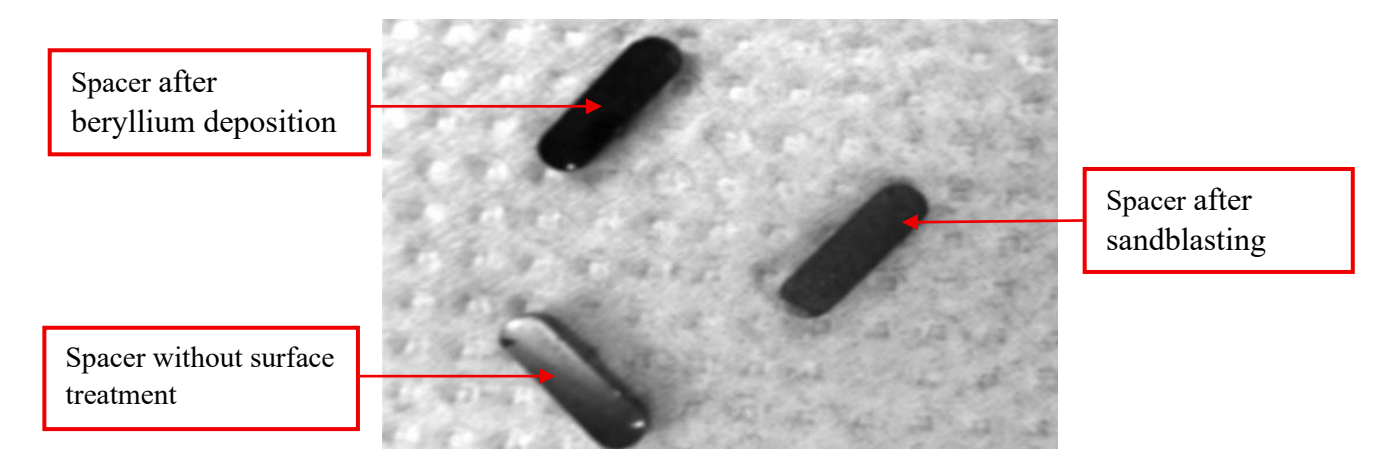


Figure 4.1: Surface morphology of spacers after sandblasting, without surface treatment, and after beryllium deposition

Figure 4.2(a) reveals localized oxidation within the brazed zone, occurring after the welding process. This oxidation indicates inadequate control of the brazing atmosphere, which can compromise the chemical and mechanical integrity of the joint formed with the cladding.

In Figure 4.2(b), a bonding defect is observed between the pad and the fuel rod cladding, resulting from an insufficient amount of beryllium. This defect highlights the critical importance of controlling the deposited quantity to ensure the formation of a continuous and reliable interface.

Conversely, **Figure 4.2(c)** illustrates an excess of beryllium, leading to an irregular excessive thickness at the brazed joint with the cladding. This excess may lead to uneven thermal distribution, porosity formation, or mechanical instability, potentially jeopardizing the structural integrity of the assembly.

These macroscopic observations confirm that the brazing quality between the pad, spacer, and Zircaloy-4 cladding depends both on the thickness of the deposited beryllium and on meticulous surface preparation.

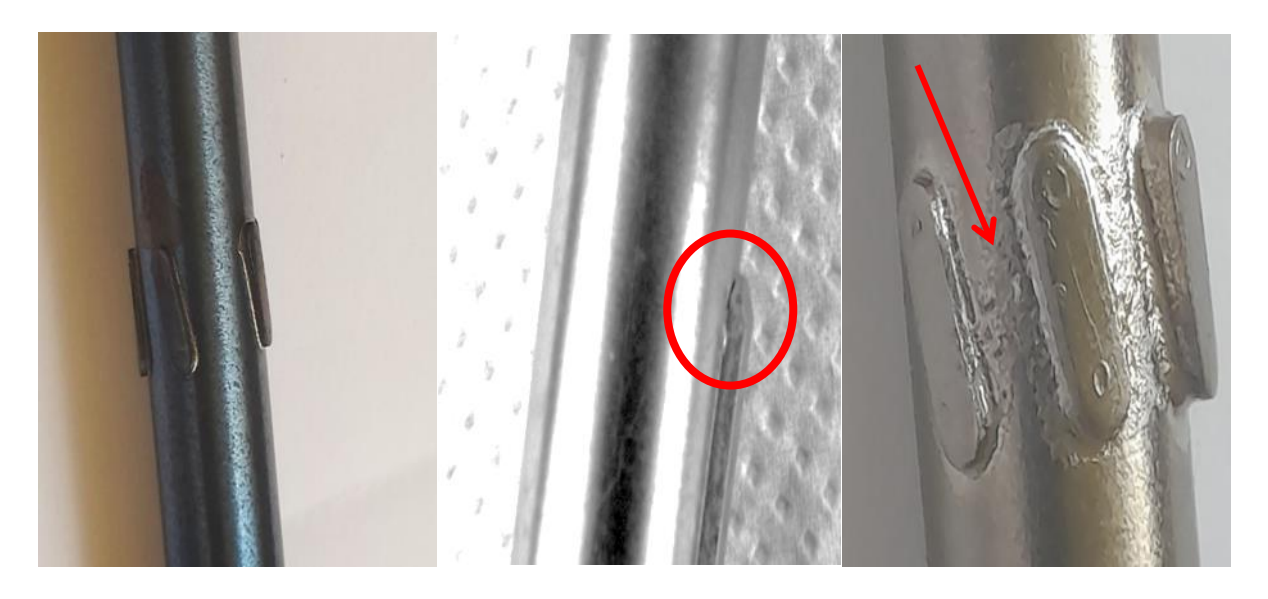


Figure 4.2: (a) Localized oxidation in the brazing zone, (b) Bonding defect, (c) Excessive beryllium at the joint

3 Microstructural Characterization

3.1 Optical Micrography

Optical micrographic analysis enabled a detailed examination of the microstructure of the Zircaloy-4 fuel rod cladding, as well as the quality of the brazed joints with the pads. These

observations are essential for evaluating the influence of the brazing process and beryllium deposition conditions on the formation of metallurgical interfaces.

Figure 4.3 presents the typical microstructure of the Zircaloy-4 cladding after brazing. A clear *Widmanstätten* structure can be observed, which is characteristic of the thermal treatments applied during the process. This morphology indicates a controlled phase transformation, resulting from a relatively slow cooling rate following the thermal cycle.

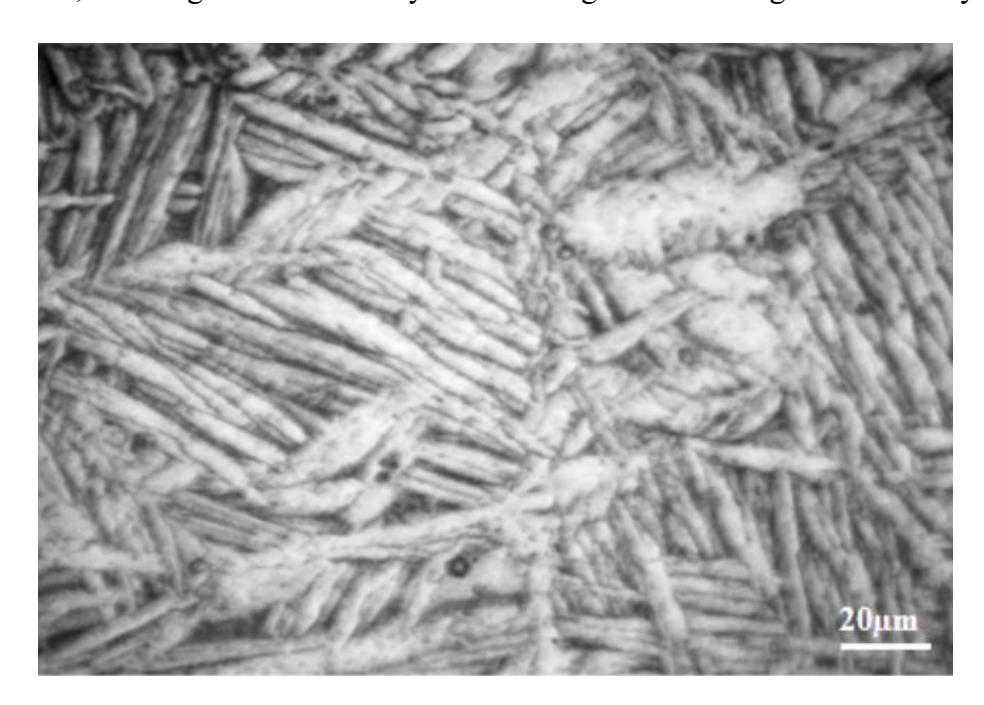


Figure 4.3: Microstructure of Zircaloy-4 cladding after brazing (*Widmanstätten* structure)

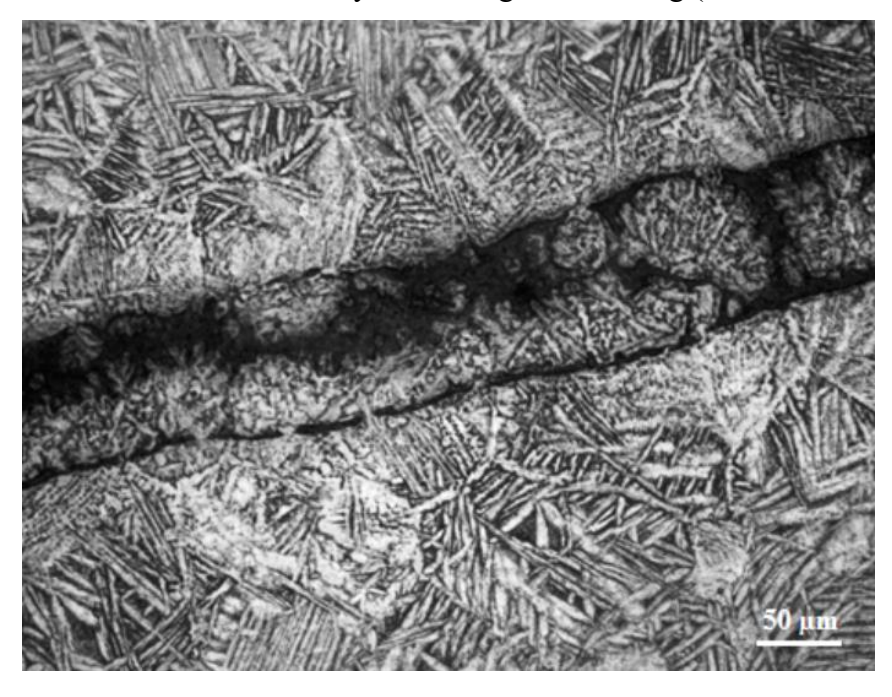


Figure 4.4: Microstructure of the brazed joint between the pad and the Zircaloy-4 cladding

Figure 4.4 illustrates the brazed joint between the pad and the cladding. A good microstructural continuity is observed, with no visible discontinuities, suggesting effective metallurgical interaction between the two materials. This indicates successful thermal brazing.

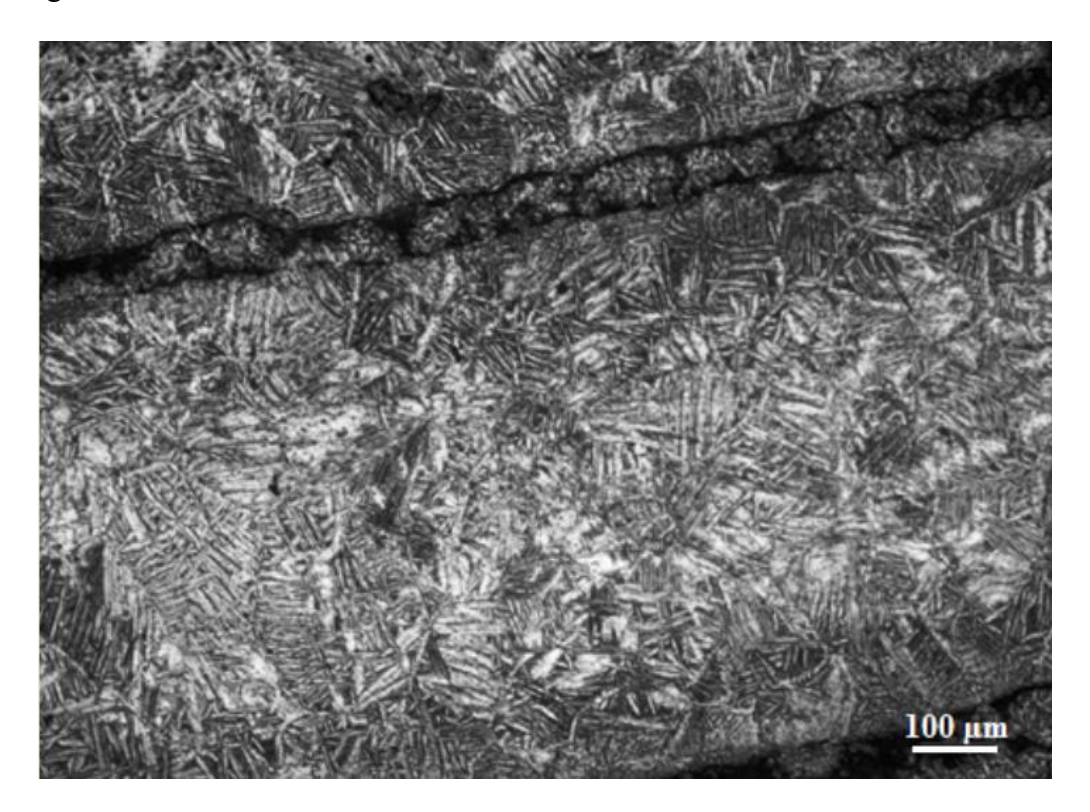


Figure 4.5: Two spacer–cladding brazed joints for two spacers

Figure 4.5 shows the microstructure of two spacer-cladding brazed joints for spacers positioned at a specific location within the fuel element. The observations reveal an overall homogeneity of the joints.



Figure 4.6: Localized porosity at the pad–cladding interface

Figure 4.6 reveals a porosity-type defect in the brazing zone. This porosity, located at the interface between the pad and the cladding, is a typical indicator of a welding issue, possibly related to an uncontrolled atmosphere, surface contamination, or poor wettability of the beryllium.

In **Figure 4.7**, another defect is observed, this time associated with an inhomogeneous beryllium deposition and insufficient thickness. The lack of brazing material leads to an incomplete joint, resulting in a clear discontinuity at the interface. This type of defect emphasizes the need for strict control over the deposition thickness prior to welding.



Figure 4.7: Welding defect due to non-uniform beryllium deposition

Finally, **Figure 4.8** highlights an excess of beryllium in the brazed joint. This surplus leads to an irregular accumulation of the material, which may introduce internal stresses or promote the formation of microcracks or weak zones within the joint.



Figure 4.8: Excess beryllium defect in the brazing zone

3.2 SEM Characterization

Figure 4.9 presents two images obtained through scanning electron microscopy (SEM), highlighting the contact zone between a spacer and a Zircaloy-4 cladding joined by beryllium brazing. The first micrograph, providing an overview, shows a continuous and uniform bond, with no visible macroscopic defects such as cracks, porosities, or delaminations. This appearance suggests good wettability of the beryllium and effective control of the applied thermal cycle [6,18].

The second image, captured at higher magnification, allows for a detailed examination of the interface structure. A gradual transition between the two materials can be observed, with no sharp boundary or signs of pronounced segregation [20,26]. This configuration indicates a well-controlled diffusion of alloying elements, particularly zirconium and beryllium, resulting in a homogeneous distribution at the microscopic scale [6,20,24].

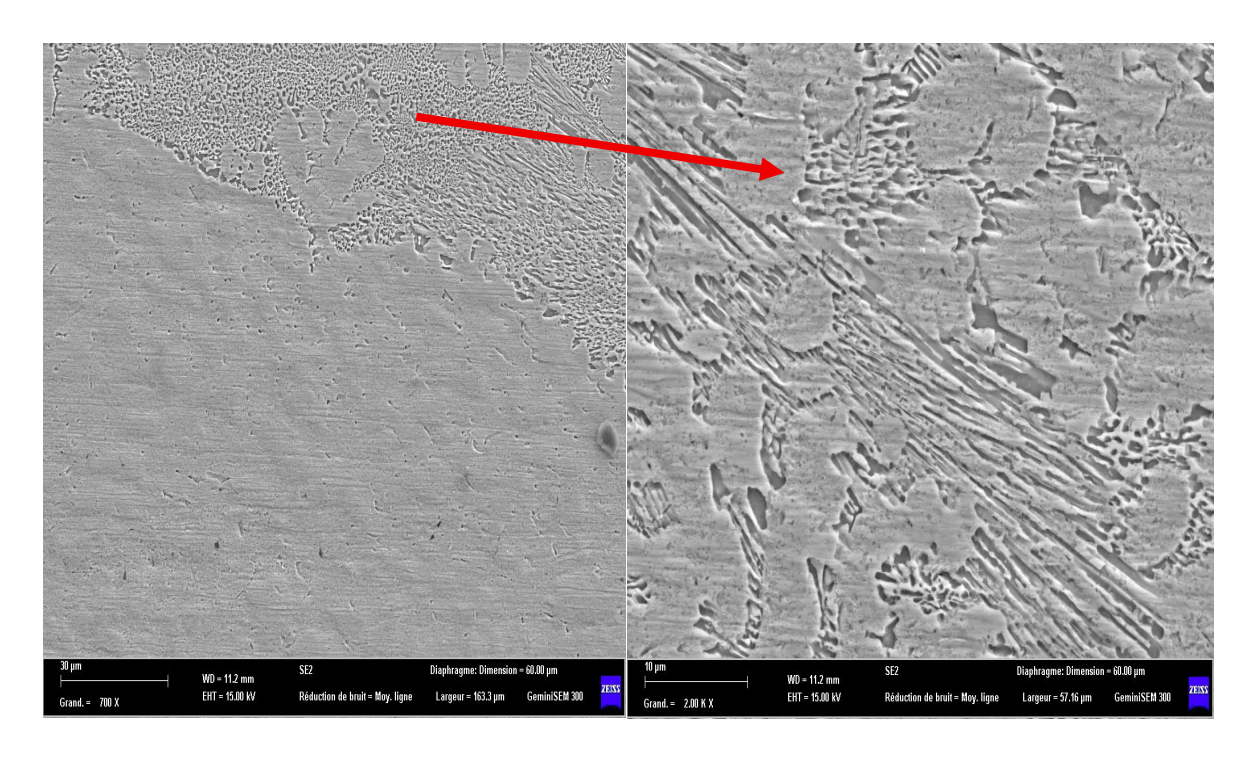


Figure 4.9: SEM microstructure of the Zr-Be brazed joint

Figure 4.10 presents a chemical mapping obtained via energy-dispersive X-ray spectroscopy (EDS) combined with scanning electron microscopy (SEM). This method enables visualization of the spatial distribution of elements within the sample. The results show a generally homogeneous distribution of both major and minor elements, suggesting effective diffusion of constituents during the brazing process [20].

From a quantitative standpoint, the sample is primarily composed of zirconium (86%), along with various alloying elements: tin (5%), chromium (4%), iron (4%), and beryllium (2%). These proportions are characteristic of a Zircaloy-4 type alloy, whose matrix is primarily zirconium enriched with typical alloying additions. The slightly lower zirconium content compared to standard values (97-98%) is likely due to the incorporation of beryllium within the brazed zone [6].

The elevated concentrations of Sn, Cr, and Fe compared to typical Zircaloy-4 values may result from local enrichment at the brazed interface, thermal treatment effects, or the use of a modified alloy variant. The significant presence of beryllium (2%) confirms its role as the brazing metal, with its diffusion into the matrix indicating effective transfer during the process [6].

Additional analysis using eZAF Smart Quant identified two distinct phases within the sample:

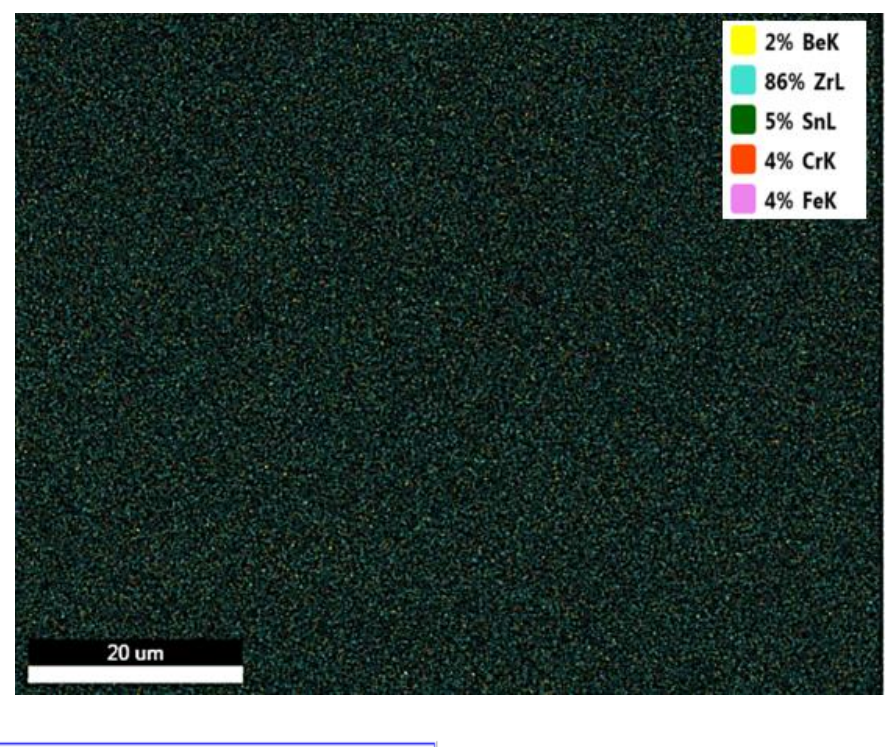
- A phase rich in zirconium (ZrL phase), also contains chromium: 96.31% Zr, 1.67% Sn, 0.43% Cr, 1.57% Fe, and 0.02% Be.
- Chromium-free phase, richer in tin: 96.34% Zr, 2.38% Sn, 1.27% Fe, and 0.01% Be.

This distinction indicates local redistribution of alloying elements particularly chromium and tin induced by the brazing process [20].

Although the presence of beryllium is clearly confirmed, its precise quantification remains challenging due to the limitations of EDS in detecting light elements. The low measured concentrations (0.01-0.02%) contrast with the initial 2%, reflecting both spatial variability in the sample and detection limits of the technique. Nevertheless, its detection remains a reliable indicator of its integration into the brazed zone [6].

The overall uniformity of elemental distribution, without signs of segregation or depletion, indicates well-controlled thermal brazing and high-quality bonding. In the nuclear field, where Zircaloy-4 is commonly used for its low neutron absorption and corrosion resistance, the use of beryllium as a brazing metal appears justified [6]. Its properties namely low neutron absorption and ability to form strong joints at moderate temperatures make it an ideal candidate.

However, the local compositional changes observed, especially in terms of chromium distribution, may affect the corrosion resistance of the joint and warrant careful consideration under actual operating conditions [24].



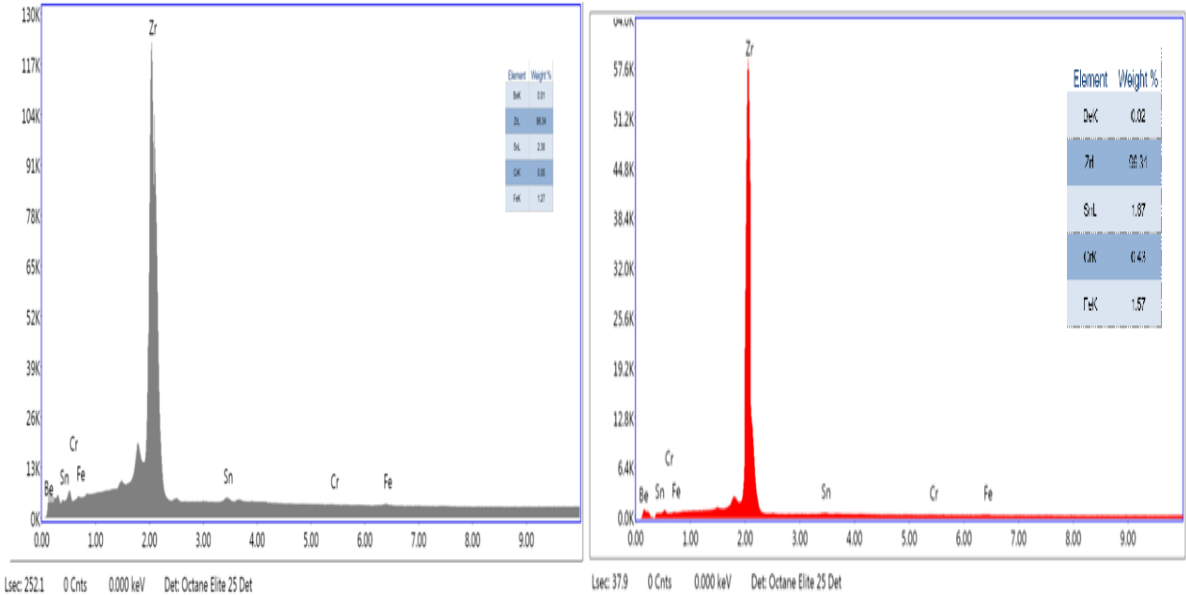


Figure 4.10: EDS chemical mapping of the Zr–Be brazed zone

Figure 4.11 Figure 4.11 shows a line scan performed using energy-dispersive X-ray spectroscopy (EDS) in conjunction with scanning electron microscopy (SEM). This analysis was conducted to observe the distribution of chemical elements within the brazed zone connecting a Zircaloy-4 type alloy to high-purity beryllium (99.9%), used as the brazing metal. The scan follows a path crossing the interface between the two materials, enabling the evaluation of chemical continuity and diffusion homogeneity at the microscopic scale.

Chapter 4: Results and Discussion

The results indicate a strong presence of zirconium in the matrix, with intensity values ranging from 5500 to 6500 counts, consistent with the expected composition of Zircaloy-4 [1]. Other alloying elements such as tin, chromium, and iron were also detected, but at significantly lower intensities (around 500 counts or less), confirming their secondary role in the alloy. Beryllium was clearly identified, with an intensity comparable to that of the minor alloying elements, indicating its effective incorporation into the brazed zone [6].

The concentration profiles along the scan line show a relatively uniform distribution of zirconium, with no abrupt breaks or visible discontinuities [20]. The other elements, including beryllium, exhibit smooth gradients without sharp transitions, suggesting efficient diffusion and good chemical transition at the interface [20]. The absence of pronounced peaks or zones of depletion or enrichment indicates that the joint is well-formed, with a gradual transition between materials, typical of a metallurgically stable assembly [20].

In conclusion, these observations validate both the conformity of the Zircaloy-4 composition [1] and the effectiveness of 99.9% pure beryllium as a brazing metal for this type of assembly [6]. The observed chemical continuity and homogeneity across the analyzed zone are promising indicators of joint quality, and thus of its mechanical performance and durability under real operating conditions [20]. This analytical method proves to be highly relevant for ensuring the reliability of such assemblies, particularly in critical applications such as those found in the nuclear field [6,20].

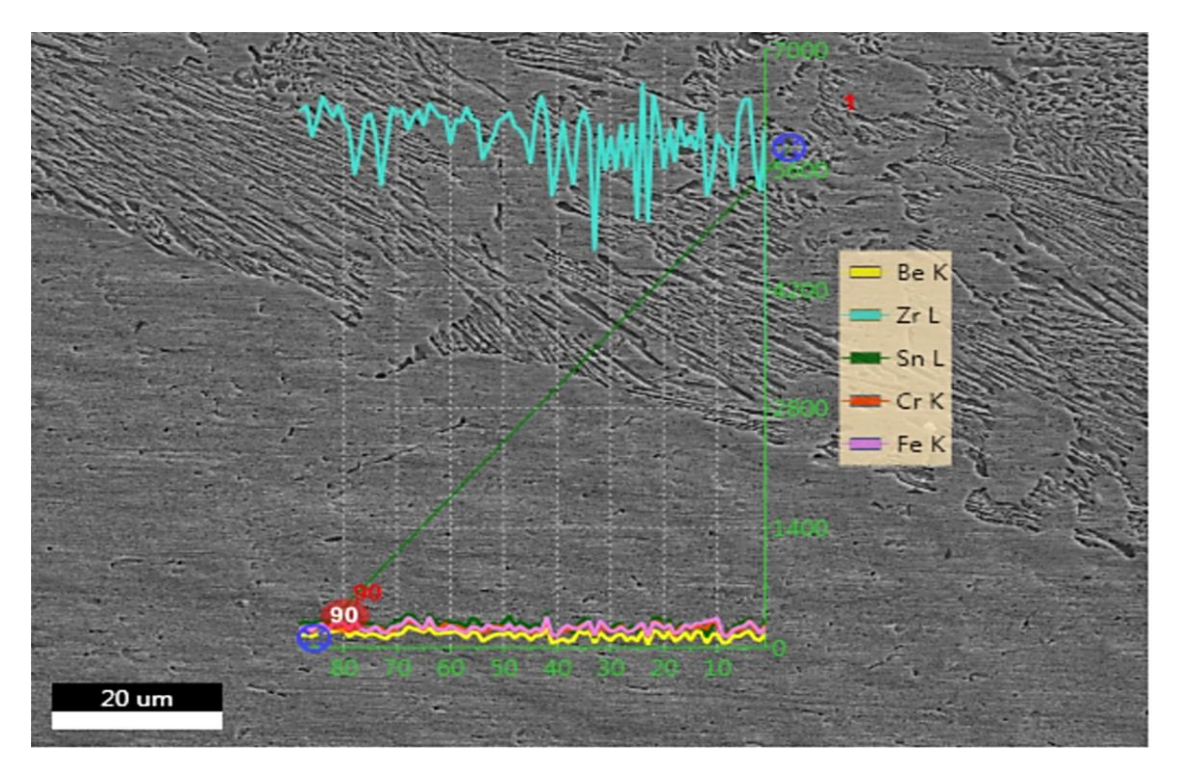


Figure 4.11: Elemental concentration profile (line scan) across the Zr–Be brazed zone

3.3 XRD Characterization

Figure 4.12 presents the results of the X-ray diffraction (XRD) analysis performed on the brazed assembly. The resulting spectrum highlights the predominant crystalline phases present in the analyzed zone, particularly those associated with Zircaloy-4. However, no beryllium-containing phases were detected.

The XRD pattern reveals the formation of several intermetallic phases, with particular emphasis on the (FeCr)₂Zr compound [20,24]. This ternary intermetallic phase represents a significant finding as it indicates the occurrence of solid-state reactions between the constituent elements during the brazing process [20]. The (FeCr)₂Zr phase belongs to the Laves phase family, characterized by a hexagonal crystal structure (space group P6₃/mmc) with lattice parameters typically around a = 4.98 Å and c = 8.15 Å [20,24].

The absence of beryllium-containing phases remains notable and is likely due to the very low beryllium content in the matrix, estimated at less than 2% [6,20]. At such low concentrations, the detection limit of XRD is exceeded, especially if beryllium is homogeneously dissolved within other phases without forming distinct intermetallic compounds [6,18]. Additionally, beryllium may have formed amorphous phases or solid solutions that are not readily detectable by conventional XRD techniques [6,20]. The limited sensitivity of this method thus prevents the clear identification of trace elements, even if they played an active role in the

metallurgical behavior at the interface, potentially acting as wetting agents or diffusion enhancers during the brazing process [6,20].

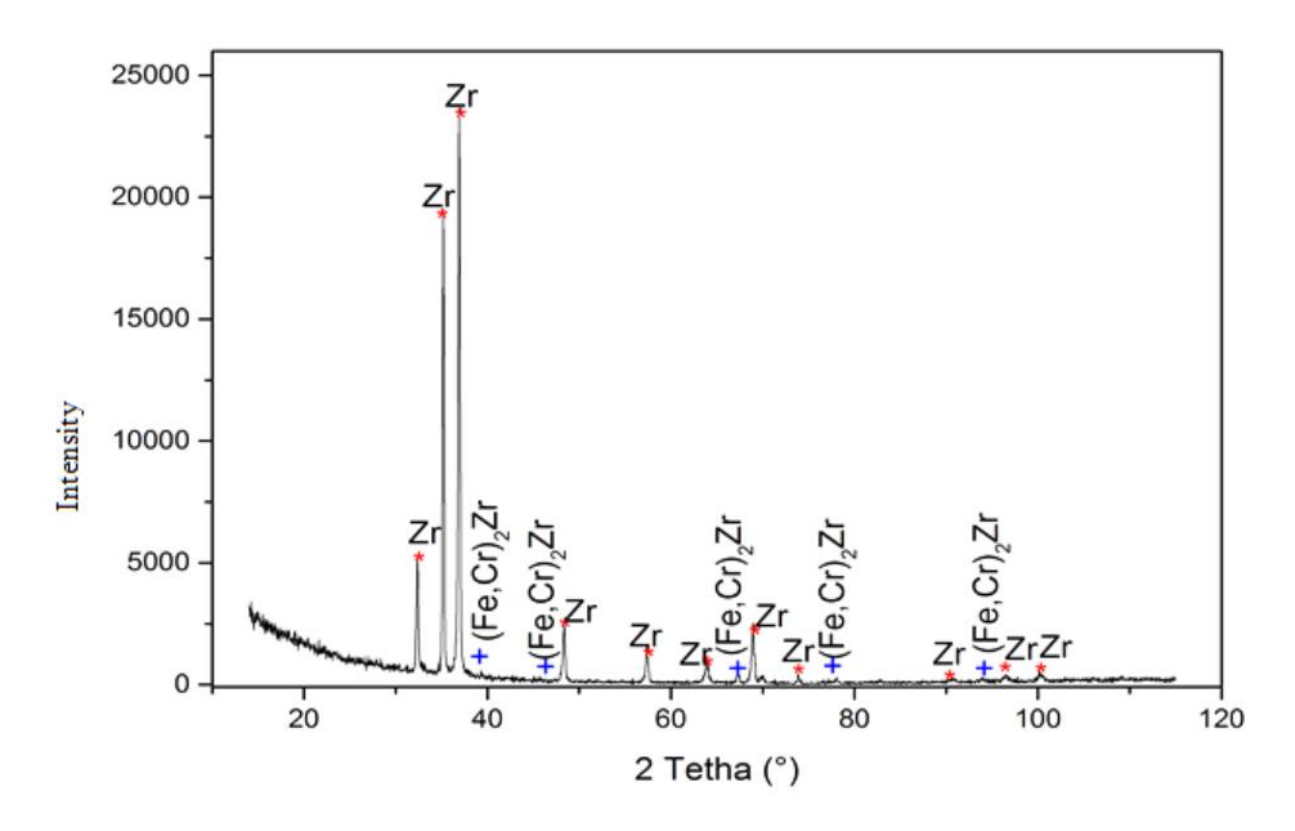


Figure 4.12: X-ray diffraction (XRD) spectrum of the brazed Zircaloy-4 sample

4 Microhardness Profile

The microhardness profile shown in Figure 13 reveals a heat-affected zone with moderate hardening in the brazed area. This increase in hardness is typical of alloying element diffusion—particularly Fe and Be into the matrix, which may induce solid solution strengthening or the local formation of fine phases. The absence of sharp hardness peaks suggests that the brazing process did not generate brittle zones, ensuring good mechanical continuity at the interface.

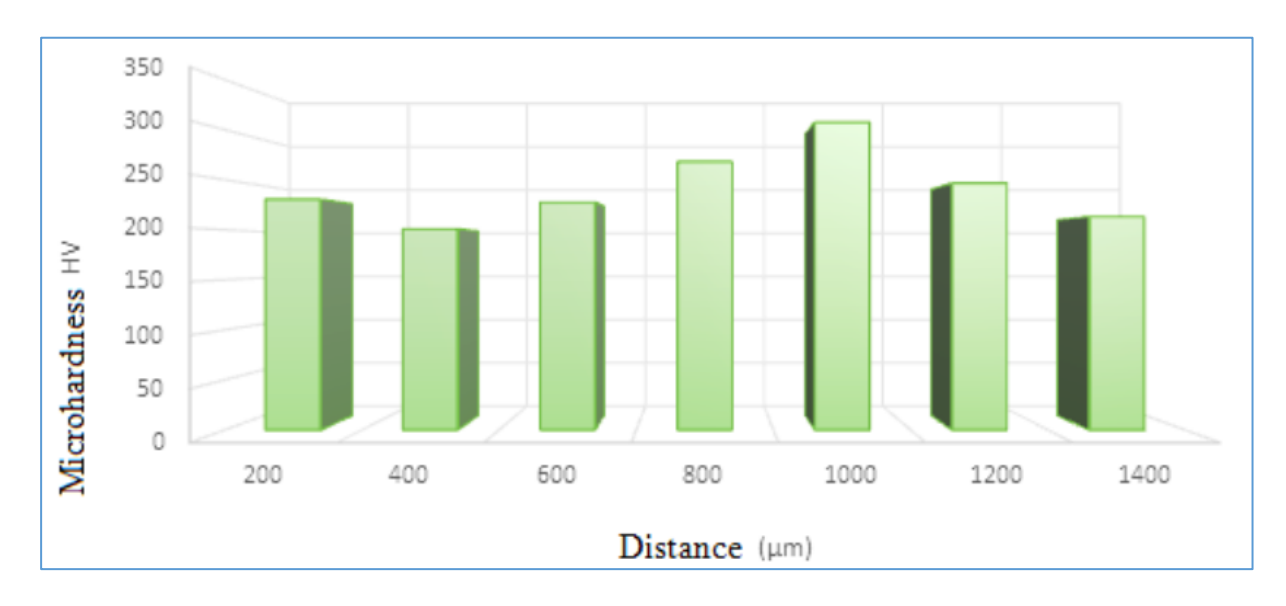


Figure 4.13: Microhardness profile of the spacer—cladding interface in Zircaloy-4 brazed with beryllium

The microhardness profile shown in Figure 14 confirms the trends previously observed, while highlighting increased joint homogeneity in the case of the double spacer configuration. The more uniform distribution of hardness values indicates a more balanced diffusion of elements across the interfaces. This mechanical stability supports the idea that the double spacer configuration optimizes the thermal conditions during brazing and reduces stress gradients an advantageous factor for long-term performance in harsh environments.

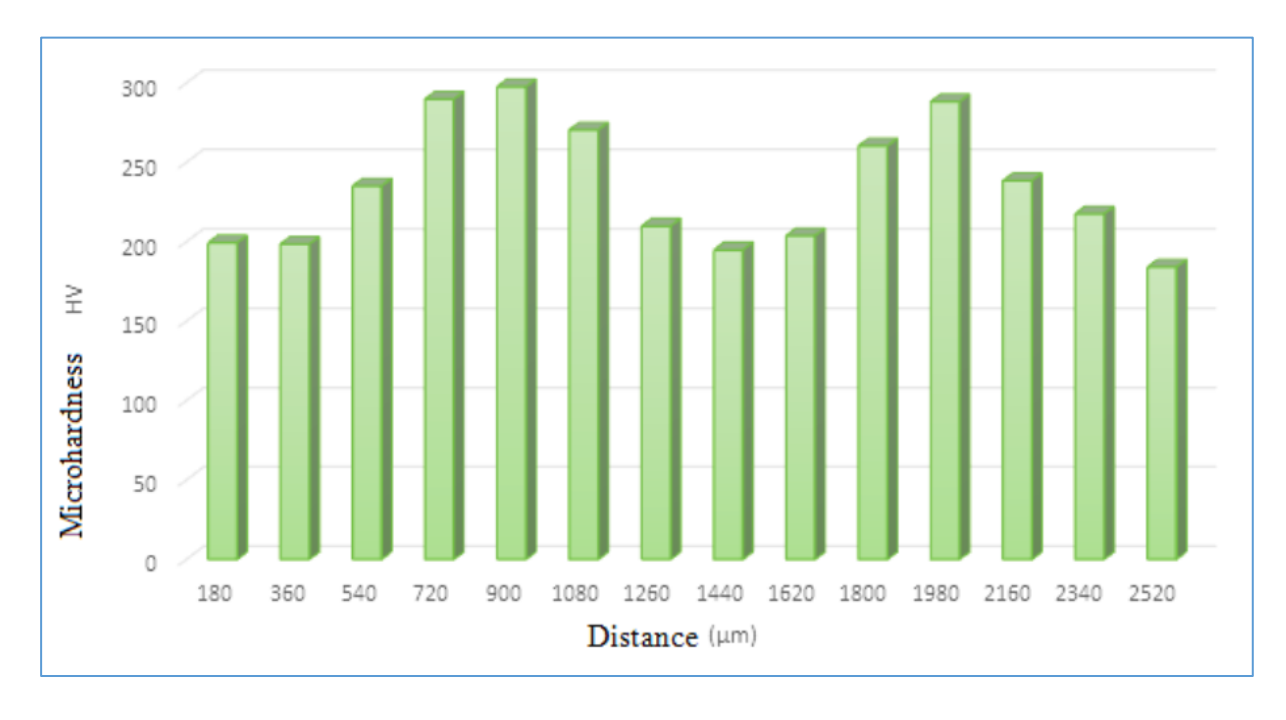


Figure 4.14: Microhardness profile for double spacers–Zircaloy-4 cladding brazed with beryllium Intensity

5 Conclusion

The results obtained throughout this study highlight the effectiveness of beryllium as a brazing metal for Zircaloy-4 assemblies, provided that surface preparation and thermal process parameters are well controlled. Microstructural analyses confirmed the formation of homogeneous and continuous interfaces, with no apparent critical defects. Elemental distribution observed through SEM/EDS indicates a balanced diffusion of alloying elements, although the accurate detection of beryllium remains limited due to its low concentration.

Microhardness profiles reveal a mechanically stable transition zone, without signs of excessive embrittlement. These findings thus confirm the potential of this type of brazed joint for applications in nuclear environment.

General Conclusion and Outlook

General Conclusion

This study is part of a broader research initiative aimed at optimizing joining techniques between metallic components used in the nuclear sector, specifically between spacers, pads, and Zircaloy-4 cladding. The primary objective was to assess the performance of beryllium as a brazing metal through an in-depth evaluation of the interface quality from microstructural, mechanical, and chemical perspectives.

The various analyses conducted yielded several significant findings. Macroscopic observations highlighted the notable influence of surface preparation—particularly sandblasting—and the thickness of the beryllium coating on the overall brazing quality. Typical defects such as oxidation, porosity, or excess material were identified and linked to specific process parameters. These findings underscore the critical importance of rigorous surface control prior to the brazing operation.

Microstructural examinations, initially performed using optical microscopy and further refined with scanning electron microscopy (SEM), revealed satisfactory continuity at the material interfaces, with no sharp discontinuities or zones of weakness. The gradual transition between Zircaloy-4 and beryllium indicates a well-controlled diffusion process, resulting in a homogeneous redistribution of elements at the microscopic scale. These results confirm the quality of the brazed joints and the metallurgical stability of the interfaces.

Chemical analysis, carried out by energy-dispersive X-ray spectroscopy (EDS) coupled with SEM, enabled the mapping of elemental distribution within the brazed region. The obtained profiles demonstrated efficient diffusion of alloying elements—including zirconium, tin, chromium, iron, and beryllium—across the interface. The observed chemical homogeneity reflects a well-managed interdiffusion process, supported by appropriate thermal conditions. The absence of significant segregation and the continuity of concentration gradients suggest a consistent solid—solid interaction, with no apparent chemical discontinuities, contributing to the mechanical integrity and long-term durability of the joint.

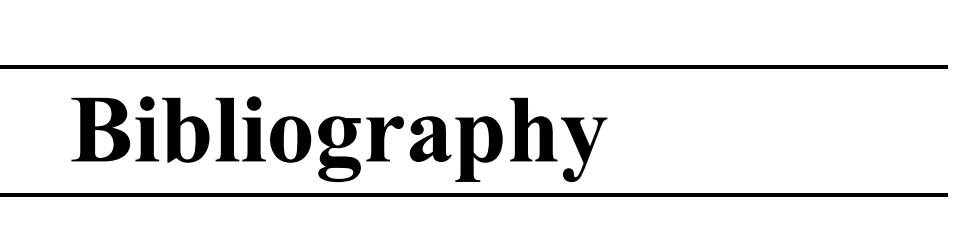
Microhardness measurements revealed a slight increase in hardness within the brazed zone, indicating diffusion of alloying elements without the formation of brittle regions. In the case of double spacers, the observed profile suggests enhanced homogenization and improved mechanical stability at the interface.

Overall, the results validate the potential of beryllium as a brazing metal for this type of application. Its low neutron absorption, high diffusivity, and ability to form robust bonds at moderate temperatures make it a promising candidate for nuclear fuel assembly components. However, precise control of each processing step remains essential to ensure consistent quality and reproducible outcomes.

Outlook and Future Work

Several research directions can be considered to further extend and deepen this study:

- 1. Optimization of the beryllium deposition process;
- 2. Advanced characterization of beryllium in the matrix using Raman spectroscopy;
- 3. Long-term aging studies of the brazed joint, including its mechanical performance and corrosion behavior;
- 4. Comparative studies with alternative brazing metals.



Bibliography

- [1] C. Lemaignan, 2.07 Zirconium Alloys: Properties and Characteristics, vol. 1–5. Elsevier Inc., 2012. doi: 10.1016/B978-0-08-056033-5.00015-X.
- [2] L. S. Foster, *The metallurgy of zirconium*, vol. 33, no. 8. 1956. doi: 10.1021/ed033p419.1.
- [3] F. C. Tubing and N. Reactors, Fracture Toughness Behavior of Zircaloy-4. 2004.
- [4] H. Olsson and J. Sundqvist, "Brazing as a Fabrication Method when Manufacturing an Intermediate Compressor Case in Stainless Steel."
- [5] I. Nazionale, "UNIVERSITA' DEGLI STUDI 'Surface Treatments for Industrial Applications' Brazing of Alumina/304 Stainless Steel for rotating joint applications," 2016.
- [6] B. A. Kalin, A. N. Suchkov, V. T. Fedotov, et al., Brazing of Be with CuCrZr-bronze using copper-based filler metal STEMET, Nuclear Materials and Energy, vol. 9, p. 388-393, 2016.
- [7] C.-D. Huang, J.-R. Hwang, et J.-Y. Huang, Optimization of vacuum brazing process parameters in Ti-6Al-4V alloy, Metals, vol. 12, no 6, p. 974, 2022.
- [8] Y. S. Cai, R. C. Liu, Z. W. Zhu, et al., Effect of brazing temperature and brazing time on the microstructure and tensile strength of TiAl-based alloy joints with Ti-Zr-Cu-Ni amorphous alloy as filler metal, Intermetallics, vol. 91, p. 35-44, 2017.
- [9] A. Rabinkin, A. E. Shapiro, et M. Boretius, Advances in Brazing: Science, Technology and Applications, 2013.
- [10] V. Fedorov, S. Weis, et G. Wagner, Mechanical and microstructural behavior of brazed aluminum/stainless steel mixed joints, dans IOP Conference Series: Materials Science and Engineering, IOP Publishing, p. 012003, 2016.
- [11] H. Tian, J. Xiong, L. Zhao, et al., Enhanced vacuum brazing joining between Ti–48Al–2Cr–2Nb/Ti–22Al–25Nb intermetallic alloys by Zr-free Ti-based filler, Journal of Materials Research and Technology, vol. 33, p. 6925-6935, 2024.
- [12] H. Bian, N. Jiang, D. Lin, et al., Microstructure and Mechanical Property of Zr/316L Brazed Joints by Zr–Cu–Fe Amorphous Filler, Metals and Materials International, vol. 30, no 6, p. 1624-1634, 2024.
- [13] R. B. Adamson, K. Coleman, S. T. Mahmood, et al., Mechanical testing of Zirconium alloys. Volume 1, ZIRAT18/IZNA13 Special Topic Report, ANT International, Mölnlycke, Sweden, 2013.
- [14] M. M. Abu-Khader, Recent advances in nuclear power: A review, Progress in Nuclear Energy, vol. 51, no 2, p. 225-235, 2009.

- [15] H.-T. Luu et N. Merkert, Investigation of solid-state diffusion bonding of Al–Cu interfaces of metal joints using molecular dynamics simulations, Results in Surfaces and Interfaces, p. 100574, 2025.
- [16] I. Sokolov, M. K. Skakov, A. Zh. Miniyazov, et al., Analysis of the beryllium stability under standard and critical operation in a fusion reactor, Eurasian J. Phys. Funct. Mater, vol. 5, p. 188-197, 2021.
- [17] A. A. Tracton, Coatings technology handbook, CRC press, 2005.
- [18] M.-d. Hou, X.-w. Zhou, et B. Liu, Beryllium oxide utilized in nuclear reactors: Part I: Application history, thermal properties, mechanical properties, corrosion behavior and fabrication methods, Nuclear Engineering and Technology, vol. 54, no 12, p. 4393-4411, 2022.
- [19] S. Simões, F. Viana, A. Sofia Ramos, et al., Microstructural characterization of diffusion bonds assisted by Ni/Ti nanolayers, Journal of Materials Engineering and Performance, vol. 25, p. 3245-3251, 2016.
- [20] Z. Wang, X. Yang, J. Wang, et al., Microstructure and mechanical properties of vacuum diffusion bonded Zr-4 alloy joint, Crystals, vol. 11, no 11, p. 1437, 2021.
- [21] M. Tupin, C. Bisor, P. Bossis, et al., Mechanism of corrosion of zirconium hydride and impact of precipitated hydrides on the Zircaloy-4 corrosion behaviour, Corrosion Science, vol. 98, p. 478-493, 2015.
- [22] Z. Li, J. Wang, et M. Ding, A review on optimization methods for nuclear reactor fuel reloading analysis, Nuclear Engineering and Design, vol. 397, p. 111950, 2022.
- [23] A. Khanolkar, T. Yao, Z. Hua, et al., In situ monitoring of microstructure evolution during thermal processing of uranium-zirconium alloys using laser-generated ultrasound, Journal of Nuclear Materials, vol. 553, p. 153005, 2021.
- [24] F. Onimus, S. Doriot, et J.-L. Béchade, Radiation effects in zirconium alloys, Comprehensive nuclear materials, vol. 3, p. 1-56, 2020.
- [25] M. A. Khattak, A. A. B. Omran, S. Kazi, et al., A review of failure modes of nuclear fuel cladding, Journal of Engineering Science and Technology, vol. 14, no 3, p. 1520-1541, 2019.
- [26] D. J. M. King, A. J. Knowles, D. Bowden, et al., High temperature zirconium alloys for fusion energy, Journal of Nuclear Materials, vol. 559, p. 153431, 2022.
- [27] Y. Ren, Fracture toughness behavior of Zircaloy-4 in the form of fuel cladding tubing in nuclear reactors, 2004.
- [28] D. L. Douglass, The metallurgy of zirconium, Atomic energy review, 1971.
- [29] F. Fagnoni, P. Trtik, J. M. Wheeler, et al., Hydrogen diffusion in zirconium cladding alloys with an inner liner as quantified by neutron radiography and nanoindentation, Journal of Nuclear Materials, vol. 584, p. 154574, 2023.



Laser Granulometric Analysis

Analysis Conditions:

1. Sample: White alumina (Al₂O₃)

2. Grade: 80-120 mesh

3. Mass: 0.5 g

4. Medium: Distilled water + dispersant

5. Ultrasound: 2 min at 40 kHz

6. Temperature: 22.3°C

7. Refractive index: 1.768 (alumina) / 1.333 (water)

8. Obscuration: 12.4%

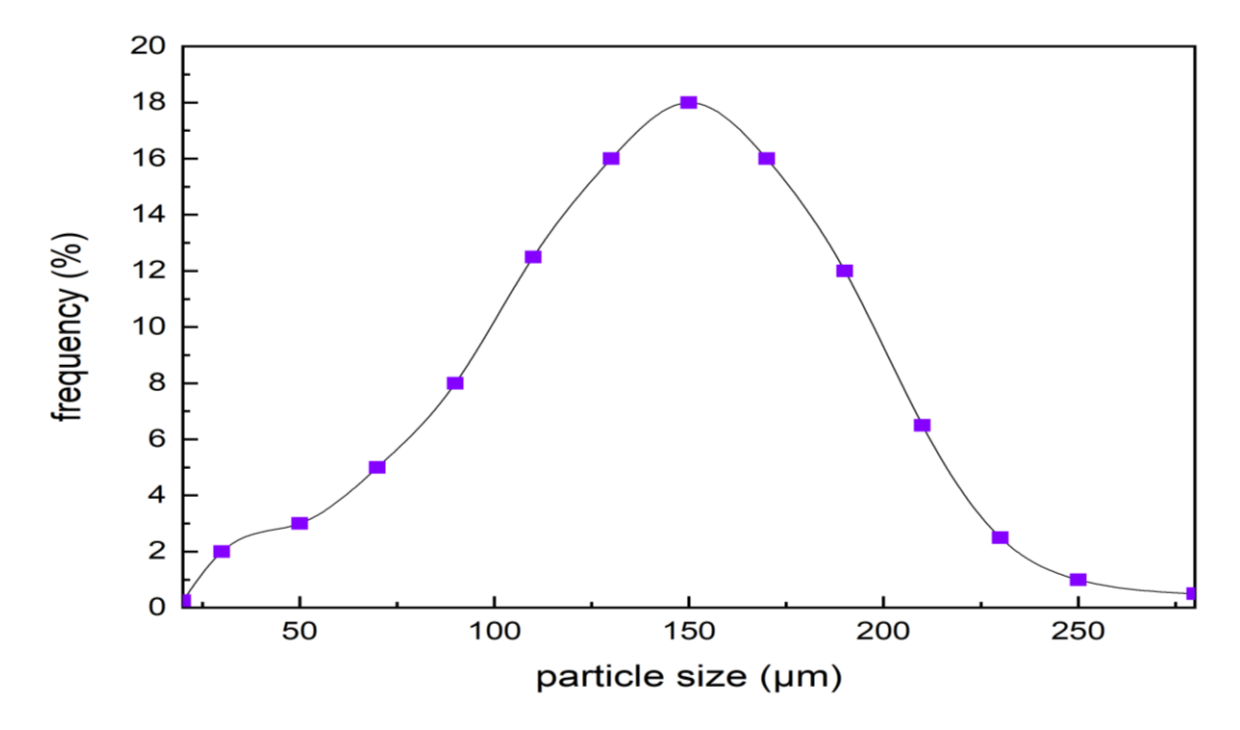


Figure 1: Differential distribution of Al₂O₃

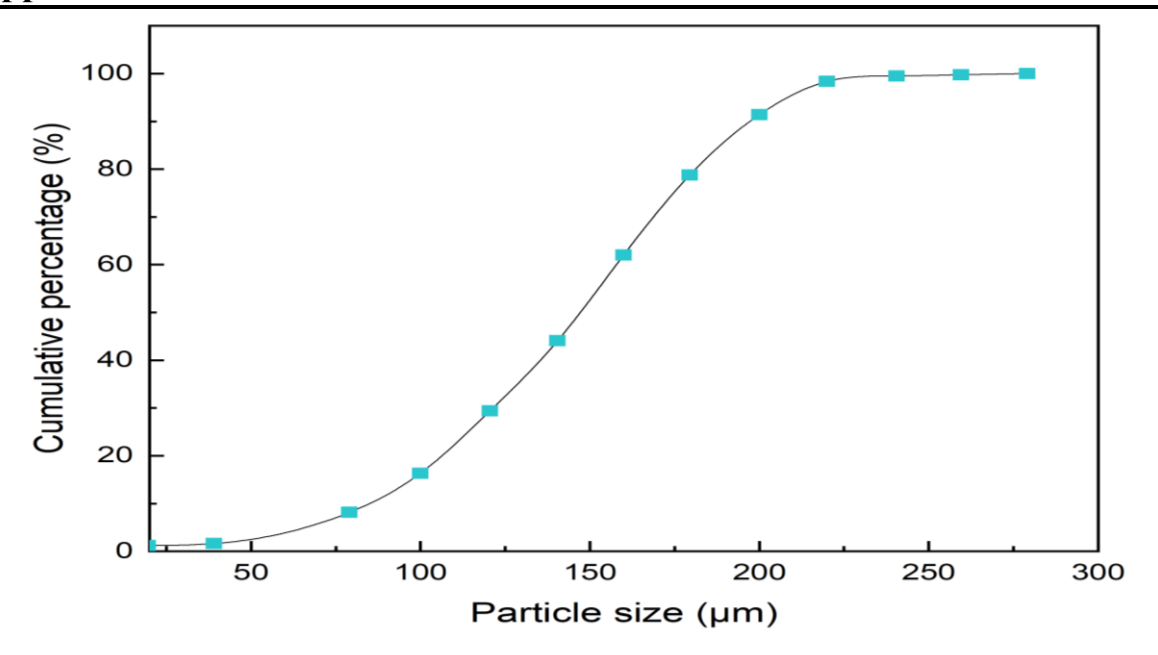


Figure 2: Cumulative distribution of Al₂O₃

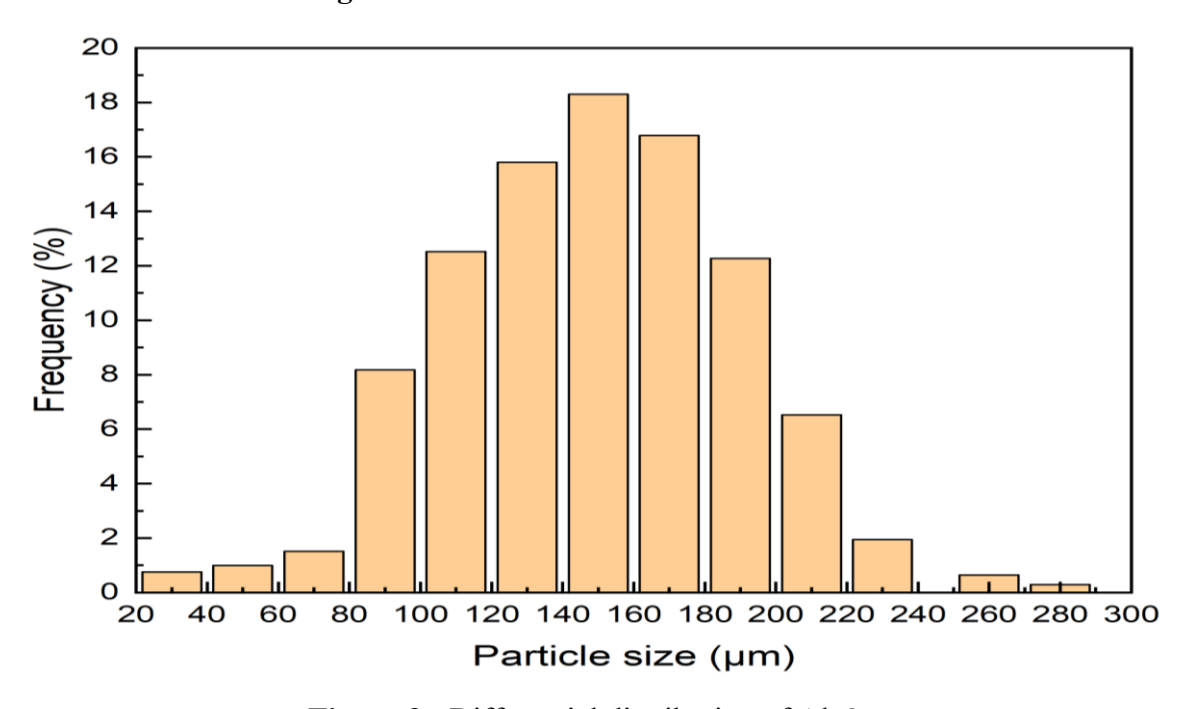


Figure 3: Differential distribution of Al₂O₃

Appendix 1

Statistical Parameters

D₁₀ (µm): 95

D50 (µm): 148

D₉₀ (μm): 195

Arithmetic mean (µm): 152

Geometric mean (µm): 144

Standard deviation (µm): 42.3

Uniformity (D90/D10): 2.05

Skewness: 0.12

Kurtosis: 2.84

Roughness measurements

The roughness of a given surface can be determined by measuring a number of parameters. Table 1, presents the most used Roughness amplitude parameters according to ISO 4287 such as Rz, Ra

Table 1: Roughness amplitude parameters according to ISO 4287

Settings	Settings	Settings	Representations	Definition					
On profiles	or	ripple							
Total	roughness.								
PROTRUSIONS and HOLLOWS									
Pp	Rp	Max (Zp i)							
PV	Rv	Wv	Max profile trough depth	Max (Zvi)v					
Pz	Pz Rz Wz		Max profile height	Max (Zp i) + Max					
				(Zvi)					
				\Rightarrow Rz = Rp + Rv					
Pc	Ground	Wc	Average height of profile elements	$\frac{1}{m}\sum_{i=1}^{m}Zt_{i}$					
	Floor			$\overline{m} \sum_{i=1}^{Z t_i}$					
PT	Rt	Wt.	Sum of the greatest of the protrusion	⇒rz					
			heights Zpi and the greatest depth of						
			the valleys Zvi (over the evaluation						
			length while the previous 4						
			parameters are determined over a						
			base length with the evaluation ≥ 1						
			base)						
		AVI	ERAGE ORDINATES						
Pa	Ra	Wa	Arithmetic mean deviation of the	$\frac{1}{l}\int_{0}^{l} Z(x) dx$					
			evaluated profile (over a base length)	$\frac{1}{l} \int_0^{l} Z(x) dx$					
			with 1 =lp; lr or lw as the case may						
			be						
PQ	Rq	Wq	RMS deviation of the evaluated	1 1					
			profile (over a base length) with 1	$\sqrt{\frac{1}{l}} \int_0^l Z^2(x) dx$					

Appendix 2

			=lp; lr or lw as the case may be	
PSK	Rsk	Wsk	Profile asymmetry factor (Skewness) defined on the amplitude distribution curve with 1 =lp; lr or lw as appropriate (lr= roughness base length)	$\frac{1}{Rq^3} \left[\frac{1}{l_r} \int_0^{l_r} Z^3(x) dx \right]$
Classical Phenylketon uria	Rku	Wku	Profile flattening factor (Kurtosis) defined on the amplitude distribution curve with 1 =lp; lr or lw as appropriate over a length of 12	$\frac{1}{Rq^4} \left[\frac{1}{l_r} \int_0^{l_r} Z^4(x) dx \right]$

In the process of manufacturing CANDU-type fuel elements, the thickness of the beryllium deposit is usually controlled using a radioactive source. In our case, this method could not be implemented. Therefore, a roughness check should be performed after sandblasting to ensure optimal adhesion of the beryllium to the substrate.

For this study, we made several roughness measurements using a tesa rugosimeter, model Rugosurf 10-G (Figure 1). This instrument is connected to a microcomputer equipped with dedicated acquisition software, allowing the automatic transfer and statistical processing of roughness data.



Figure 1: TESA-rugosurf 10-G



Figure 2: Rugosoft 10-10G Software Interface

We carried out four (04) tests on Pads, the results obtained are recorded in Table 2

Table 2: Quantities relating to the roughness measurement.

	Ra	Rq	Rt	Rz	Rp	Rv	Rsk	Rku
Pad 1	0.659	0.902	7.980	5.561	2.237	-	-	4.878
						3.324	0.451	
Pad 2	0.543	0.747	8.466	4.646	1.559	-	-	5.277
						3.086	0.845	
Pad 3	0.662	0.963	9.269	7.164	2.414	-	-	4.137
						4.750	0.569	
Pad 4	0.644	0.808	2.554	1.488	0.644	-	-	3.711
						0.844	0.389	

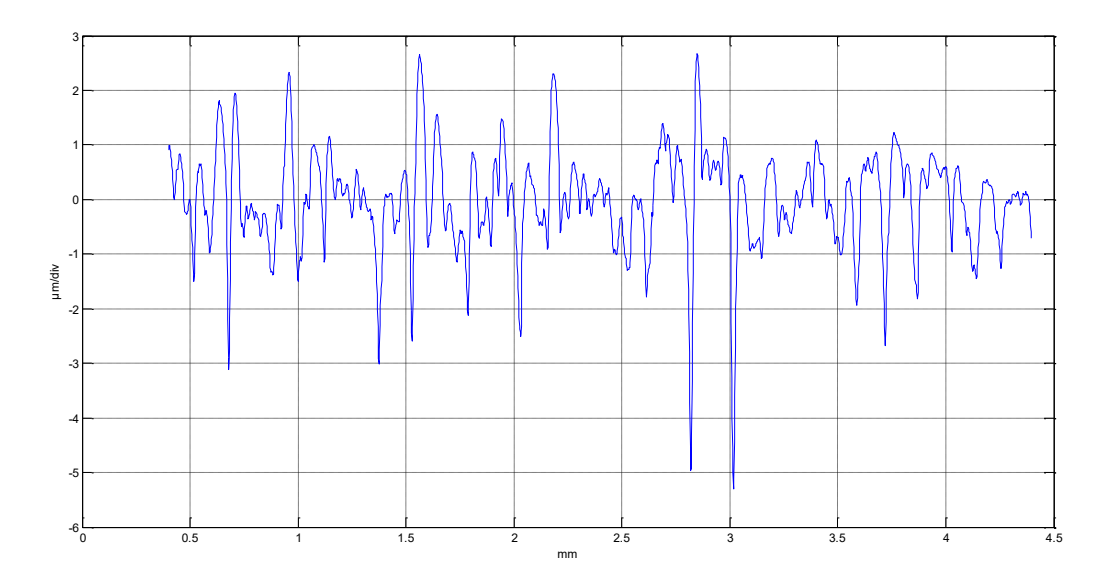


Figure 3: Roughness profile - Pad No. 1

Beryllium Toxicity

1. Introduction

Beryllium (Be) is a lightweight, brittle metal used extensively in aerospace, nuclear reactors, electronics, and manufacturing due to its high stiffness, thermal stability, and conductivity. Despite these advantages, beryllium exposure poses serious health risks, particularly in occupational settings. This appendix explores the toxicological profile, health effects, mechanisms, diagnosis, treatment, and regulatory considerations related to beryllium toxicity.

2. Chemical and Physical Properties

- Atomic number: 4
- Atomic weight: 9.0122
- Appearance: Steel gray, brittle metal
- Common forms: Metallic beryllium, beryllium oxide (BeO), beryllium alloys
- Solubility: Poorly soluble in water but soluble in acids, which can increase bioavailability and toxicity.

3. Exposure Sources and Routes

- Occupational Exposure: Mining, refining, alloy production, machining, recycling, and manufacturing of beryllium-containing products.
- **Environmental Exposure:** Generally low-level, through contaminated soil or water near industrial sites.
- **Routes:** Primarily inhalation of dust or fumes; dermal contact can cause sensitization; ingestion is rare but possible.

4. Toxicokinetics

- Inhaled beryllium particles deposit in the lungs, where soluble forms dissolve and enter cells, while insoluble particles persist, causing chronic inflammation.
- Beryllium can accumulate in lung tissue, lymph nodes, and bones.
- The metal has a long biological half-life, contributing to prolonged immune activation.

5. Health Effects

5.1 Acute Beryllium Disease

- Occurs after high-level exposure (rare today).
- Symptoms: Acute chemical pneumonitis, cough, chest pain, dyspnea, fever, weight loss.
- Pathology: Lung inflammation with alveolar damage.

5.2 Chronic Beryllium Disease (CBD)

- Immune-mediated granulomatous lung disease.
- Develops after sensitization, which can occur at low exposure levels.
- Symptoms: Chronic cough, progressive dyspnea, fatigue, weight loss, night sweats, and fever.
- Diagnosis: Confirmed by beryllium lymphocyte proliferation test (BeLPT) on blood or bronchoalveolar lavage cells, chest imaging showing granulomas or fibrosis, and lung biopsy if needed.
- Prognosis: Variable; some patients stabilize, others progress to respiratory failure.

5.3 Beryllium Sensitization

- Asymptomatic immune response detectable by BeLPT.
- Sensitized individuals are at risk of developing CBD.

5.4 Carcinogenicity

- Classified as Group 1 carcinogen by IARC.
- Epidemiological evidence links beryllium exposure to increased lung cancer risk, especially in workers with chronic exposure.

6. Mechanism of Toxicity

- Beryllium acts as a hapten, binding to self-proteins and triggering a T-helper 1 (Th1) cell-mediated immune response.
- This leads to macrophage activation, granuloma formation, and fibrosis in lung tissue.
- Genetic factors, such as HLA-DP alleles, influence susceptibility.

7. Diagnosis and Monitoring

- Beryllium Lymphocyte Proliferation Test (BeLPT): Detects sensitization by measuring lymphocyte proliferation in response to beryllium.
- Imaging: Chest X-rays and high-resolution CT scans to detect granulomas and fibrosis.
- Pulmonary Function Tests: Assess lung impairment.
- **Biopsy:** Lung tissue examination may be necessary for definitive diagnosis.

8. Treatment and Management

- Avoidance of further exposure is critical.
- Corticosteroids are the mainstay treatment to reduce inflammation and slow disease progression.
- Supportive care includes oxygen therapy and pulmonary rehabilitation.
- Lung transplantation may be considered in end-stage disease.

9. Regulatory Standards and Prevention

- Occupational exposure limits vary by country; for example, OSHA's permissible exposure limit (PEL) is $0.2 \mu g/m^3$ for beryllium dust and fumes.
- Engineering controls (ventilation, dust suppression), personal protective equipment (respirators, gloves), and medical surveillance programs are essential to prevent sensitization and disease.
- Worker education and exposure monitoring are critical components of prevention.

10. Conclusion

Beryllium toxicity represents a significant occupational health concern due to its potential to cause severe lung disease and cancer. Understanding its toxicology, mechanisms, and preventive measures is essential for protecting exposed populations.